

# Physical Properties of Iron in the Inner Core

Gerd Steinle-Neumann,<sup>1,\*</sup> Lars Stixrude,<sup>1</sup> and R. E. Cohen<sup>2</sup>

<sup>1</sup>*Department of Geological Sciences, University of Michigan, Ann Arbor, MI 48109-1063*

<sup>2</sup>*Geophysical Laboratory, Carnegie Institution of Washington, Washington, DC 20015-1035*

(Dated: June 1, 2018)

The Earth's inner core plays a vital role in the dynamics of our planet and is itself strongly exposed to dynamic processes as evidenced by a complex pattern of elastic structure. To gain deeper insight into the nature of these processes we rely on a characterization of the physical properties of the inner core which are governed by the material physics of its main constituent, iron. Here we review recent research on structure and dynamics of the inner core, focusing on advances in mineral physics. We will discuss results on core composition, crystalline structure, temperature, and various aspects of elasticity. Based on recent computational results, we will show that aggregate seismic properties of the inner core can be explained by temperature and compression effects on the elasticity of pure iron, and use single crystal anisotropy to develop a speculative textural model of the inner core that can explain major aspects of inner core anisotropy.

PACS numbers:

## INTRODUCTION

The presence and slow growth of Earth's inner core is one of the most significant manifestations of the dynamics in the interior of our planet. As it is inaccessible to direct observation, an understanding of the physical state of the inner core requires an integrative approach combining results from many fields in the geosciences. Seismology, geo- and paleomagnetism, geo- and cosmochemistry, geodynamics, and mineral physics have advanced our knowledge of the structure and processes in the inner core, revealing many surprises.

Foremost among these have been the discoveries of anisotropy and heterogeneity in the inner core. Long assumed to be a featureless spherically symmetric body, a higher number and higher quality of seismic data revealed that the inner core is strongly anisotropic to compressional wave propagation [Morelli *et al.*, 1986; Woodhouse *et al.*, 1986]. Generally, seismic waves travel faster along paths parallel to the Earth's polar axis by 3-4% compared to equatorial ray paths [Creager, 1992; Song and Helmberger, 1993]. The presence of anisotropy is significant because it promises to reveal dynamical processes within the inner core.

Anisotropy is usually attributed to lattice preferred orientation, which may develop during inner core growth [Karato, 1993; Bergman, 1997], or by solid state deformation [Buffett, 2000]. The source of stress that may be responsible for deformation of the inner core is unknown, although several mechanisms have been proposed [Jeanloz and Wenk, 1988; Yoshida *et al.*, 1996; Buffett 1996; 1997; Karato, 1999; Buffett and Bloxham 2000].

An understanding of the origin of inner core anisotropy will require further advances in our knowledge of the physical properties of iron at inner core conditions, and may rely critically on further observations of the detailed structure of the inner core. For example, recent obser-

vations indicate that the magnitude of the anisotropy may vary with position: heterogeneity has been observed on length scales from 1-1000 km [Creager, 1997; Tanaka and Hamaguchi, 1997; Vidale and Earle, 2000]. Inner core structure may change with time as well. Song and Richards [1996] interpreted apparent changes in travel times of inner core sensitive phases in terms of superrotation of the inner core with respect to the mantle. Some recent studies have argued for a much slower rotation rate than that advocated originally, or questioned the interpretation of time dependent structure [Souriau, 1998; Laske and Masters, 1999; Vidale and Earle, 2000].

The inner core also plays an essential role in the dynamics of the overlying outer core. The anisotropy and long magnetic diffusion time of the inner core may alter the frequency and nature of reversals, and influence the form of the time-averaged field [Hollerbach and Jones, 1993; Clement and Stixrude, 1995]. Moreover, important energy sources driving the geodynamo process are associated with solidification of the inner core: the density contrast across the inner core boundary is due to the phase transition from the liquid to the solid, and chemical differentiation during the incongruent freezing of the inner core. Both of these processes provide energy for the dynamo through the release of latent heat [Verhoogen, 1961] and the generation of chemical buoyancy [Braginsky, 1963]. Other energy sources for magnetic field generation are secular cooling of the Earth, gravitational energy from thermal contraction of the core, radioactive heat generation, and precession [Verhoogen, 1980; Buffett *et al.*, 1996].

Both thermal and compositional contributions to the buoyancy depend on the thermal state of the core. The more viscous mantle controls the cooling time scale of the Earth and facilitates the formation of a thermal boundary layer at the core mantle boundary. The heat flux out of the core controls the rate of inner core growth and light

element partitioning during this process [Buffett *et al.*, 1996]. Conversely, a reliable estimate on temperature in the Earth's core would advance our understanding of the current thermal state and evolution of the Earth [Jeanloz and Morris, 1986; Yukutake, 2000] with important implications for the dynamics of the Earth.

Because the inner core is inaccessible, the study of model systems by theory and experiments is essential. Here we consider the ways in which mineral physics may lend deeper insight into inner core processes and to the origin of its structure, extending previous reviews by Jeanloz [1990] and Stixrude and Brown [1998]. We begin with geophysical background on the inner core including recent seismological advances, constraints on the composition, thermal state, and dynamics of the inner core. As our subsequent discussions draw on various experimental and theoretical approaches in mineral physics we then give an overview of recent developments in methods in the following section, focusing on computational mineral physics (a recent review focusing on advances in experiments has been given by Hemley and Mao [2001]). To the extent that the inner core is composed of nearly pure iron, physical properties of this element at high pressure and temperature govern the behavior of the inner core; we consequently review advances in our knowledge of the high pressure physical properties of iron, focusing on crystalline structure, equation of state, and elasticity at both static condition and high temperature. In the final section we examine the implications of these results for inner core temperature, and integrate aspects of elasticity with considerations of the dynamics in the inner core to develop a simple speculative model of polycrystalline structure that explains major aspects of its anisotropy.

## GEOPHYSICAL BACKGROUND

### Aggregate Seismic Properties

Lehmann [1936] discovered the inner core by recognizing weak arrivals of PKiKP within the P-wave shadow zone of the core. The amplitudes of these arrivals were sufficient to invoke a discontinuous seismic boundary in the Earth's core. The P-wave contrast across this boundary was soon established; Birch [1940] and Bullen [1946] argued that the inner core must be solid based on this estimate. The best evidence for inner core solidity comes from studies of inner core sensitive normal modes [Dziewonski and Gilbert, 1971]: Earth models with finite shear modulus of the inner core provide a significantly better fit to eigenfrequency observations than those with a liquid inner core. Recent observations of body wave phases involving a shear wave in the inner core (PKJKP, SKJKP, and pPKJKP) [Okal and Cansi, 1998; Deuss *et al.*, 2000] support solidity, but are still controversial.

The inferred shear wave velocity  $v_S$  of the inner core is remarkable: it is low compared to the compressional wave velocity  $v_P$ , a property which can also be expressed in terms of the Poisson's ratio  $\sigma$ . The value of  $\sigma=0.44$  for the inner core is nearly that of a liquid (0.5), leading to speculation that this region may be partially molten [Singh *et al.*, 2000].

In principle density  $\rho$ ,  $v_P$ , and  $v_S$  also depend on depth. However, constraints on the depth dependence of  $\rho$  and  $v_S$  are weak. Seismic observations are consistent with an inner core in a state of adiabatic self-compression.

### Anisotropy

First evidence for deviations from a spherically symmetric structure came from the observation that eigenfrequencies of core sensitive normal modes are split much more strongly than predicted by ellipticity and rotation of the Earth alone [Masters and Gilbert, 1981]. Anomalies in PKIKP travel times were initially interpreted as topography on the inner core [Poupinet *et al.*, 1983]. Morelli *et al.* [1986] and Woodhouse *et al.* [1986] interpreted similar observations of eigenfrequencies and travel times as inner core anisotropy. Observation of differential travel times PKIKP-PKP<sub>BC</sub> [Creager, 1992; Song and Helmberger, 1993] and a reanalysis of normal mode data [Tromp, 1993] confirmed that the inner core displays a hexagonal (cylindrical) pattern of anisotropy with a magnitude of 3-4% and symmetry axis nearly parallel to Earth's rotation axis. For example, PKIKP arrives 5-6 s earlier along polar paths than predicted from radially symmetric Earth models such as PREM [Dziewonski and Anderson, 1981]. It is worthwhile pointing out that some of the travel time differences could be due to mantle structure not accounted for in the reference model [Bréger *et al.*, 1999; Ishii *et al.*, 2002a; 2002b]. In particular, small scale heterogeneity in the lowermost mantle could be sampled preferentially for select body wave core paths [Bregér *et al.*, 1999; Tromp, 2001; Ishii *et al.*, 2002b].

In further investigation deviations from first order anisotropy have been put forward, for example lateral variations in  $v_P$  of the inner core on length scales ranging from hemispherical differences [Tanaka and Hamaguchi, 1997; Creager, 1999; Niu and Wen, 2001], to hundreds of kilometers [Creager, 1997], down to a few kilometers [Vidale and Earle, 2000]. Radial variations may also exist: weak anisotropy may be present in the uppermost inner core (to a depth of 50-100 km) [Shearer, 1994; Song and Helmberger, 1995; Su and Dziewonski, 1995] and strong uniform anisotropy in its inner half [Song and Helmberger, 1995; Creager, 1999]. Seismological studies of the inner core are discussed in more detail elsewhere in this volume.

## Composition

Seismically determined properties of the core may be compared to laboratory measurements under high compression. Measurements of the equation of state show that only elements with an atomic number close to that of iron satisfy the seismic constraints [Birch, 1964]. Additional arguments are necessary to uniquely implicate iron [Jeanloz, 1990]: iron is one of the most abundant elements in stars and meteorites, much more so than in the portions of the Earth that are directly observable [Brown and Mussett, 1993]; and a conducting liquid is necessary in the outer core to explain the existence of a long lived dynamo process that creates Earth’s magnetic field [Merrill et al., 1996].

To the degree that we are certain about the main constituent of the core we are also sure that the core contains other lighter elements: pure iron can not satisfy the seismological constraints for both portions of the core. Liquid iron is about 10% too dense to satisfy both the density and bulk modulus in the outer core [Birch., 1964; Jeanloz, 1979; Brown and McQueen, 1986] and while solid iron can explain the bulk modulus of the inner core for reasonable temperatures it overestimates the density even for very high temperature (8000 K) [Jephcoat and Olson, 1987; Stixrude et al., 1997]. The identity and amount of the light element is still uncertain, but based on cosmochemical arguments hydrogen, carbon, oxygen, magnesium, silicon, and sulfur have been proposed [Poirier, 1994], with oxygen and sulfur being the most popular. To infer information on the composition of the core from geochemistry, two questions are of central importance: did the core form in chemical equilibrium [Karato and Murthy, 1997] and what are the physical conditions of the core forming event, as pressure and temperature critically determine the partition coefficient of various elements between silicate and metallic melt [Ito et al., 1995; Li and Agee, 1996; Okuchi, 1997].

Alternatively, one may use the available seismological information on the current physical state of the outer and inner core ( $\rho$ ,  $v_P$ ,  $v_S$ ) and compare to the physical properties of candidate iron alloys at the appropriate pressure and temperature condition. The compositional space of Fe-X with X any light element has been sparsely sampled in shock wave experiments at the conditions relevant for the core. Only binary compounds in the Fe-S system (pyrrhotite  $\text{Fe}_{0.9}\text{S}$  [Brown et al., 1984, troilite  $\text{FeS}$  [Anderson and Ahrens, 1996], and pyrite  $\text{Fe}_2\text{S}$  [Ahrens and Jeanloz, 1987; Anderson and Ahrens, 1996]) as well as wüstite  $\text{FeO}$  [Jeanloz and Ahrens, 1980; Yagi et al., 1988] have been exposed to shock. The data has been extrapolated to inner core conditions [Stixrude et al., 1997] and compared to the required elastic parameters (Fig. 1). This analysis indicates that small amounts of either S or O (few atomic percent) would be sufficient to match the

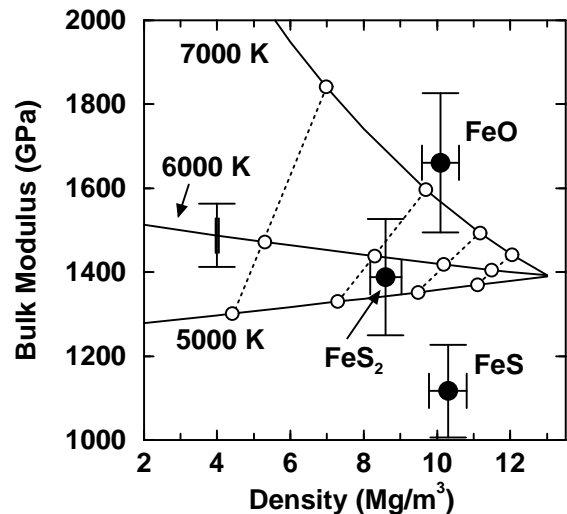


FIG. 1: Properties of the alloy fraction that are required to match the seismically observed properties of the inner core [Stixrude et al., 1997]. For a given temperature (solid lines) the required effective bulk modulus is plotted as a function of required effective density. The dashed lines connect points of common alloy fraction for any light element X (2, 5, 10, and 20% from left to right). Estimated uncertainties in the alloy fractions required are indicated with the error bars on the curve corresponding to 6000 K (1% in density and 5% in bulk modulus). Superimposed are extrapolations of shock wave experimental estimates for FeO [Jeanloz and Ahrens, 1980; Yagi et al., 1988], FeS [Anderson and Ahrens, 1996], and  $\text{Fe}_2\text{S}$  [Ahrens and Jeanloz, 1987; Anderson and Ahrens, 1996] at 345 GPa and 6000 K (estimated uncertainties are 5% in density and 10% in bulk modulus).

properties of the inner core.

Alfè et al. [2000a; 2000b; 2002] combined the geophysical approach with a chemical argument. They evaluated the liquid-solid partition coefficients of candidate light elements assuming thermodynamic equilibrium at the inner core boundary. The results show that neither S, Si, nor O alone can satisfy the observed density contrast at the inner core boundary and that a ternary or higher mixture of small amounts of S or Si with O is required.

## Thermal State

Like the composition, the temperature of the inner core cannot be determined by direct observation. Assuming that the inner core is growing in equilibrium from incongruent freezing of the outer core liquid a knowledge of the melting behavior of iron-rich systems at the pressure of the inner core boundary (330 GPa) would yield an important fixed-point temperature for the construction of whole Earth geotherms. Because the core is not a pure system, the temperature at the inner core boundary should differ from the melting point of pure iron. Freez-

ing point depression in an eutectic system with no solid solution is given by the van Laar equation [Brown and McQueen, 1982] which yields a value of 800 K for a melting point of iron of 6000 K and 10% mole fraction of the light element. The value for the freezing point depression must be viewed as highly uncertain, however, since solid solution almost certainly exists at the high temperatures of the core. An independent estimate of the temperature of the core may be obtained by comparing the elastic properties of iron with those seismologically determined. We describe this approach as applied to the inner core below.

Seismic observations do provide constraints on some aspects of the thermal state of the core. In the outer core the compressional wave velocity  $v_P$  equals the bulk sound velocity  $v_B = \sqrt{K_S/\rho}$ . In a homogeneous, convecting system,  $v_B$  and  $\rho$  are related by adiabatic self-compression. Deviations from this state are characterized by the Bullen [1963] inhomogeneity parameter  $\eta$  being different from one.  $\eta$  is defined as

$$\eta = -\frac{v_B^2}{\rho g} \frac{\partial \rho}{\partial r}, \quad (1)$$

where  $g$  the gravitational acceleration, and  $r$  the radius.  $\eta$  for the outer core is constrained by seismology to be  $1 \pm 0.05$  [Masters, 1979]. This is consistent with (but does not uniquely require) a vigorously convecting outer core, and a resulting geotherm close to an adiabat, characterized by the gradient:

$$\frac{\partial T}{\partial r} = -\frac{\gamma g}{v_B^2} T, \quad (2)$$

where  $\gamma$  is the Grüneisen parameter. Adopting the value measured for liquid iron at core conditions ( $\gamma=1.5$ ) [Brown and McQueen, 1986] and a temperature at the inner core boundary of 6000 K, one finds a temperature contrast of 1500 K across the outer core.

The temperature contrast in the inner core is likely to be small. We can place an upper bound on it by assuming that the inner core is a perfect thermal insulator. If the inner core grows through freezing of the outer core its temperature profile will follow the solidus temperature. Based on this assumption *Stixrude et al.* [1997] estimated the total temperature difference across the inner core to be less than 400 K. Conductive or convective heat loss will further reduce this temperature gradient relative to the insulating case. Conduction is likely to be a very effective way to extract heat from the inner core, such that the temperature profile may fall below an adiabat [Yukutake, 1998; Buffett, 2000].

### Dynamics

*Song and Richards* [1996] found that the differential travel time of PKIKP-PKP<sub>BC</sub> for earthquakes in the

South Sandwich islands recorded in Alaska increased by 0.3 s over a period of three decades, and concluded that the inner core rotates relative to the mantle by  $1^\circ$ /year, a finding that was confirmed qualitatively using global data sets [Su et al., 1996]. *Creager* [1997] showed that part of the signal could be explained by lateral heterogeneity in the inner core, and reassessed the rotation rate to a lower value. Recent years have seen body wave [Souriau, 1998] and free oscillations studies [Laske and Masters, 1999] that can not resolve inner core rotation, and put close bounds on rotation rate.

If it is present, differential inner core rotation would provide one of the few opportunities for direct observations of the dynamics in Earth's deep interior. Moreover, differential rotation could have a significant effect on the angular momentum budget of the Earth yielding an explanation of decadal fluctuations in the length of day [Buffett, 1996; Buffett and Creager, 1999]. Its origin is not fully understood, but geodynamo simulations produce super-rotation by electro-magnetic coupling with the overlying outer core [Glatzmaier and Roberts, 1996; Kuang and Bloxham, 1997; Aurnou et al., 1998]. Gravitational stresses, arising from mass anomalies in the mantle, are also expected to act on the inner core [Buffett, 1996; 1997]. These tend to work against super-rotation by gravitationally locking the inner core into synchronous rotation with the mantle. In detail, the interplay between forces driving and resisting super-rotation depend on the rheology of the inner core, which is currently unknown. If the viscosity is sufficiently low, super-rotation may take place, with the consequence that the inner core undergoes continuous viscous deformation in response to the gravitational perturbations.

The interaction of super-rotation with gravitational stresses is just one of many proposed sources of internal deformation in the inner core. The subject has received substantial attention because solid state flow in the inner core can result in lattice-preferred orientation, thought to be essential for producing seismically observed anisotropy.

Other proposed sources of stress in the inner core include:

(a) Coupling with the magnetic field generated in the overlying outer core [Karato, 1999; Buffett and Bloxham, 2000; Buffett and Wenk, 2001]. Karato [1999] considered the radial component of the Lorentz force ( $F_r$ ) at the inner core boundary which is caused by the zonal magnetic field ( $B_\phi$ ). This is typically the strongest contribution to the Lorentz force in geodynamo models [Glatzmaier and Roberts, 1995; Kuang and Bloxham, 1997]. Buffett and Bloxham [2000] argue that the inner core adjusts to  $F_r$  in a way to minimize steady solid state flow: only weak flow in the inner core is induced that is largely confined to the outermost portion. Considering additional terms to the Lorentz force  $\vec{F}$  by including radial components of the magnetic field  $B_r$  they conclude that the azimuthal

term  $F_\phi$  which is proportional to  $B_r B_\phi$  induces a steady shear flow throughout the inner core.

(b) Thermal convection [Jeanloz and Wenk, 1988; Wenk et al., 2000a]. As in any proposed model of inner core flow, the viscosity of the inner core remains an important uncertainty, as does the origin and magnitude of heat sources required to drive the convection.

(c) Aspherical growth of the inner core [Yoshida et al., 1996]. Fundamental considerations, based on the expected cylindrical symmetry of flow in the outer core, and detailed geodynamo simulations [Glatzmaier and Roberts, 1995] indicate that heat is transported more efficiently in the equatorial plane than along the poles, leading to an inhomogeneous growth rate of the inner core, and internal viscous relaxation. A key question is whether the magnitude of the effect is sufficient to produce lattice preferred orientation. In particular, the resulting strain rates are very small, and may not be sufficient to generate significant polycrystalline texture via recrystallization.

It has also been proposed that polycrystalline texture in the inner core may be acquired during solidification [Karato, 1993; Bergman, 1997]. However, if the inner core does experience solid state deformation, by one or more of the mechanisms described above, it is unclear to what extent the texture acquired during solidification would be preserved. It is possible that texture in the outermost portions of the inner core is dominated by the solidification process, whereas lattice preferred orientation in the bulk of the inner core is produced by deformation.

Further progress in our understanding of the composition, temperature, dynamics, and origin of anisotropy in the inner core is currently limited by our lack of knowledge of the properties of iron and iron alloys at high pressures and temperatures. A better understanding of elastic and other properties of iron at inner core conditions can provide a way to test hypotheses concerning the state and dynamics of the inner core.

## MINERAL PHYSICS METHODS

As elasticity plays a central role in deep Earth geophysics we will emphasize aspects of mineral physics that are directly related to the determination of elastic properties. To gain deeper insight into complex elastic behavior, such as anisotropy, we need to know the full elastic constant tensor at the conditions in the Earth's center. We will focus on methods based on first-principles quantum mechanical theory, but also briefly review experimental progress, as it relates to comparison and validation of theory. A full review of experimental work has been given recently by Hemley and Mao [2001].

## Experimental Progress

Determination of the elastic constants of metals in the diamond cell remains a particular challenge as now-standard techniques, such as Brillouin spectroscopy, cannot readily be used for opaque materials. A variety of alternative methods have been developed and applied to study iron at high pressure and ambient temperature. In the lattice strain technique [Singh et al., 1998a; 1998b] X-ray diffraction is used to study the strain induced in a polycrystal by uniaxial stress. A full determination of the elastic constant requires the measurement of  $d$ -spacing for many  $(h, k, l)$  lattice planes, or additional assumptions such as homogeneity of the stress field in the sample [Mao et al., 1998]. Other efforts have exploited the relationship between phonon dispersion in the long-wavelength limit and elastic wave propagation: measurements of phonon dispersion have been used to estimate the average elastic wave velocity [Lübbbers et al., 2000; Mao et al., 2001], and the longitudinal wave velocity [Fiquet et al., 2001]. An approximate calibration has been explored in which the zone-center Raman active optical mode is related to the  $c_{44}$  shear elastic constant by a Brillouin-zone folding argument [Olijnyk and Jephcoat, 2000]. Finally, Anderson et al. [2001] by analyzing pressure induced changes in the intensity of X-ray diffraction patterns from hcp iron, extracted a Debye temperature  $\Theta_D$ , and thus average elastic wave velocity, which they equated with  $v_S$ .

Whereas diamond anvil cell experiments most readily measure properties at ambient temperature, shock wave experiments achieve pressure and temperature conditions similar to those of the core through dynamic compression. By varying the speed of the driver impacting the sample, a set of different thermodynamic conditions are accessed, along a curve in pressure-density space called the Hugoniot. Temperature is not determined directly by the Rankine-Hugoniot equations, it must be measured using special techniques, such as optical pyrometry [Yoo et al., 1993] or calculated on the basis of a thermodynamic model [Brown and McQueen, 1986]. Using temperature and Grüneisen parameter an adiabatic bulk modulus ( $K_S$ ) on the Hugoniot can be determined. The impact of the driver plate on the sample not only sets up a shock in the sample but also in the plate itself. When the shock wave reflects off the back of the impactor, pressure is released and a longitudinal (compressional) sound wave is set up traveling forward through the system of impactor and sample. This has been exploited to determine  $v_P$ ; combining  $v_P$  with  $K_S$  the corresponding  $v_S$  can be calculated [Brown and McQueen, 1986].

## Computational Mineral Physics

With the sparse probing of thermodynamic conditions relevant for Earth's inner core by the experimental methods discussed in the previous section, and the difficulty to obtain information on single crystal elasticity, first-principles material physics methods provide an ideal supplement to experimental study, with all of thermodynamic space accessible, and various approaches to determine elasticity at hand. In the following sections we will introduce the basic principles of calculating such properties.

### Total Energy Methods

Density functional theory [Hohenberg and Kohn, 1964; Kohn and Sham, 1965] provides a powerful and in principle exact way to obtain the energetics of a material with  $N$  nuclei and  $n$  interacting electrons in the ground-state (for a review see Lundqvist and March [1987]), with the electronic charge density  $\rho_e(\vec{r})$  being the fundamental variable. It can be shown [Hohenberg and Kohn, 1964] that ground state properties are a unique functional of  $\rho_e(\vec{r})$  with the total (internal) energy

$$E[\rho_e(\vec{r})] = T[\rho_e(\vec{r})] + U[\rho_e(\vec{r})] + E_{xc}[\rho_e(\vec{r})]. \quad (3)$$

Here  $T$  is the kinetic energy of a system of non-interacting electrons with the same charge density as the interacting system, and  $U$  is the electrostatic (Coulomb) energy containing terms for the electrostatic interaction between the nuclei, the electrons, and nuclei-electron interactions. The final term  $E_{xc}$  is the exchange-correlation energy accounting for many body interactions between the electrons. Density functional theory allows one to calculate the exact charge density  $\rho_e(\vec{r})$  and hence the many-body total energy from a set of  $n$  single-particle coupled differential equations [Kohn and Sham, 1965]

$$\{-\nabla^2 + V_{KS}[\rho_e(\vec{r})]\}\psi_i = \varepsilon_i\psi_i, \quad (4)$$

where  $\psi_i$  is the wave function of a single electronic state,  $\varepsilon_i$  the corresponding eigenvalue, and  $V_{KS}$  the effective (Kohn-Sham) potential that includes the Coulomb and exchange-correlation terms from (3). The Kohn-Sham equations are solved self-consistently by iteration. Density functional theory has been generalized to spin polarized (magnetic) systems [Singh, 1994].

While density functional theory is exact in principle the exact solution of the Kohn-Sham equations requires the knowledge of the universal form of the exchange-correlation potential which is yet unknown. Approximations for  $V_{xc}$  however have been very successful. The local density approximation (LDA) [Lundqvist and March, 1983] replaces  $V_{xc}$  at every point in the crystal with the value of a homogeneous electron gas with the same local

charge density. This lowest order approximation yields excellent agreement with experiment for a wide variety of materials, but fails for some metals. Most prominently for iron LDA wrongly predicts hcp as the ground state structure for iron at ambient pressure [Stixrude *et al.*, 1994]. Generalized gradient approximations (GGA) include a dependence on local gradients of the charge density in addition to the charge density itself [Perdew *et al.*, 1996]. GGA yields the correct ground state of iron at ambient pressure and predicts the phase transition from bcc to hcp iron at the experimentally determined pressure [Asada and Terakura, 1992; Stixrude *et al.*, 1994].

In addition to total energy it is possible to calculate directly first derivatives of the total energy with first-principles methods. This allows one to determine forces acting on the nuclei and stresses acting on the lattice [Nielsen and Martins, 1985].

All-electron, or full potential methods make no additional essential approximations to density functional theory. Computational methods such as the Linearized Augmented Plane Wave (LAPW) method provide an important standard of comparison. All-electron methods are very costly (slow), and are currently impractical for many problems of interest. More approximate computational methods have been developed, which, when applied with care, can yield results that are nearly identical to the all-electron limit.

In the pseudopotential approximation the nucleus and core electrons are replaced inside a sphere of radius  $r_c$  (cut-off radius) with a simpler object that has the same scattering properties (for a review see Pickett [1989]). The pseudopotential is much smoother than the bare Coulomb potential of the nuclei, and the solution sought is only for the pseudo-wavefunctions of the valence electrons that show less rapid spatial fluctuations than the real wavefunction in the core region or those of the core electrons themselves. The construction of the pseudopotential is non-unique and good agreement with all-electron calculations must be demonstrated.

Iron provides a particular challenge. For example, all-electron results show that pressure-induced changes in the  $3p$  band are important for the equation of state [Stixrude *et al.*, 1994], and so should be treated fully as valence electrons in a pseudopotential approach.

For our work on the high temperature elasticity of hcp iron [Steinle-Neumann *et al.*, 2001] we have constructed a Troullier-Martins [Troullier and Martins, 1991] type pseudopotential for iron in which  $3s$ ,  $3p$ ,  $3d$ , and higher electronic states are treated fully as valence electrons. Agreement with all-electron calculations of the equation of state and elastic constants is excellent: for hcp iron the pressure at inner core densities is within 1 % of all-electron (LAPW) results (Fig. 2), and the elastic constant tensor at inner core density is within 2% rms.

The predictions of density functional theory can be compared directly with experiment, or with geophysical

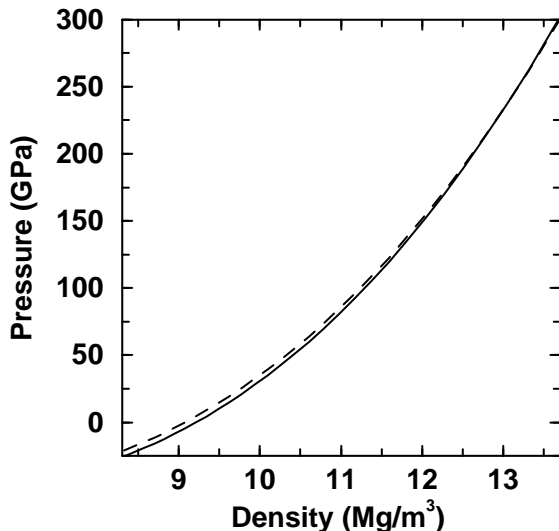


FIG. 2: Equation of state for hcp iron obtained from all electron results (dashed line) [Steinle-Neumann *et al.*, 1999] and the pseudopotential used in the calculation of high temperature thermoelasticity (solid line) [Steinle-Neumann *et al.*, 2001].

observations. For example, by computing the total energy as a function of volume, one obtains the equation of state. This equation of state is static, that is the effects of thermal vibrations are absent. This athermal state is one that is not attainable in the lab where zero-point motion cannot be eliminated. Static properties are often directly comparable to experimental measurements taken at ambient temperature since the effect of 300 K is small for properties such as the density, or the elastic constants. However, for comparison with the earth's core, thermal effects are essential. Calculation of the effects of temperature from first-principles is more involved because one must calculate the energies associated with atomic displacements, including those that break the symmetry of the lattice.

### High Temperature Methods

Statistical mechanics provides the tools to deal with material properties at high temperature. The thermodynamic behavior of any physical system is uniquely defined by the so-called fundamental relation, which, for a non-magnetic or Pauli-paramagnetic solid in the canonical ensemble (particle number  $N$ , volume  $V$ , and temperature  $T$  held constant) takes the form

$$F(V, T) = E(V, T) - TS_{el}(V, T) + F_{vib}(V, T) \quad (5)$$

where  $F$  is the Helmholtz free energy. The total energy  $E(V, T)$  is now a function of  $T$  as well, because we explicitly have to account for thermal excitation of electrons

according to Fermi-Dirac statistics.  $S_{el}$  is the entropy associated with this excitation of the electrons [McMahon and Ross, 1977], and  $F_{vib}$  is the vibrational part of the free energy.  $F_{vib}$  is derived from the partition function for a system with  $N$  atoms, which in the classical limit, appropriate at high temperature conditions (significantly above  $\Theta_D$ ) is

$$Z_{vib} = \frac{1}{N! \Lambda^{3N}} \cdot \int d\vec{R}_1 d\vec{R}_2 \dots d\vec{R}_N \exp \left[ -\frac{F_{el}(\vec{R}_1, \vec{R}_2, \dots, \vec{R}_N; T)}{kT} \right] \quad (6)$$

and

$$F_{vib} = -kT \ln Z_{vib}. \quad (7)$$

$Z_{vib}$  is a  $3N$  dimensional integral over the coordinates of the nuclei located at  $\vec{R}_i$  with the electronic free energy  $F_{el} = E - TS_{el}$  uniquely defined by the coordinates of the atoms and  $T$ .  $\Lambda = h/\sqrt{2\pi mkT}$  is the de Broglie wavelength with  $h$  the Planck and  $k$  the Boltzmann constant, and  $m$  the nuclear mass.

A naïve attempt to evaluate the integral (7) fails because of the large dimensionality, and because most configurations contribute little to the integral. What is required is a search of configuration space that is directed towards those configurations that have relatively low energy. In the particle-in-a-cell (PIC) method and the lattice dynamics method described next, atoms are restricted to vibrations about their ideal crystallographic sites, that is diffusion is neglected. This is not a severe approximation to equilibrium thermodynamic properties at temperatures below the premelting region. Molecular dynamics, described last, in principle permits diffusion, although in practice computationally feasible dynamical trajectories are sufficiently short that special techniques are often required to study non-equilibrium processes.

### Particle-in-a-Cell

Here the basic approximation motivates the division of the lattice into non-overlapping sub-volumes centered on the nuclei (Wigner-Seitz cell  $\Delta_{ws}$ ) with the coordinates of each atom restricted to its cell. A second basic assumption in the PIC model is that the motions of the atoms are uncorrelated. We can expect this approximation to become increasingly valid with rising temperature above  $\Theta_D$  and below melting.

If the energy change resulting from moving one particle be independent of the vibrations of the other atoms, the partition function factorizes, and the  $3N$  dimensional integral is replaced by the product of  $N$  identical 3-dimensional integrals, which reduces the computational burden tremendously

$$Z_{vib} = \frac{1}{\Lambda^{3N}} \left( \int_{\Delta_{ws}} d\vec{R}_w \exp \left[ \frac{-\Delta F_{el}(\vec{R}_w, T)}{kT} \right] \right)^N \quad (8)$$

with

$$\Delta F_{el}(\vec{R}_w, T) = F_{el}(\vec{R}_w, T) - F_{el}(\vec{R}_{w0}, T). \quad (9)$$

( $N!$  no longer appears in the prefactor of (8) as the atoms are distinguished by their lattice site.) One evaluates the energetics of moving one atom  $w$  (the so-called wanderer) with the equilibrium lattice position  $\vec{R}_{w0}$  in the potential of the otherwise ideal lattice; this is a mean field approach to the vibrational free energy.

Because large displacements of  $w$  are included in the integral (up to about 1/2 nearest neighbor distance) the PIC model treats anharmonicity of the vibrations explicitly. The method is computationally very efficient, and can be sped up even more by minimizing the total number of calculations involved in evaluating the integral (8). The angular integrations can be performed efficiently by developing a quadrature which requires evaluation of the integrand along a small number of special directions that are determined by the point symmetry of the lattice site [Wasserman *et al.*, 1996].

The cell model has been used for calculations on iron for the thermodynamics of both the hcp and fcc phase [Wasserman *et al.*, 1996], and for high temperature elasticity of hcp iron [Steinle-Neumann *et al.*, 2001]. It has also been successfully applied to thermoelasticity of tantalum [Cohen and Gülseren, 2001; Gülseren and Cohen, 2002].

### Lattice Dynamics

The calculation of forces on the atoms allows one directly to compute the vibrational frequencies of the material. The dynamical matrix may be calculated row by row by displacing one atom by a small amount from its equilibrium site in a supercell and evaluating the resulting forces on the other atoms.  $F_{vib}$  is then calculated by performing the appropriate summation over wavevector and phonon branches.

A fundamental approximation in lattice dynamics is that the vibrations of the atoms about their equilibrium are harmonic, only terms that are quadratic in atomic displacements are retained in the expression for the total energy. However, anharmonicity might become important for conditions of the inner core where the temperature is just below the melting point of the material, and considerable effort must be put into anharmonic corrections.

Lattice dynamics has been used extensively over the past few years to address the thermodynamics of hcp iron [Alfè *et al.*, 2001], studies on stability of various phases [Vočadlo *et al.*, 2000], melting [Alfè *et al.*, 1999], and studies on core composition [Alfè *et al.*, 2000a; 2000b; 2002].

While lattice dynamics and the PIC model essentially evaluate ensemble averages for the thermodynamics of a system, molecular dynamics explores the time evolution of a single realization of the system. In this case thermodynamic properties are calculated as time averages by appealing to the ergodic hypothesis. To obtain the time evolution of the system the forces acting on the atoms are coupled with Newton's second law. The set of  $N$  coupled differential equations is then integrated. A large supercell (100 atoms) and long time series (thousands of time steps) are required for convergence of equilibrium properties. Molecular dynamics has been applied to the study of high temperature properties of solid iron including melting [Laio *et al.*, 2000] by using a clever hybrid scheme for the electronic structure, as well as for liquid iron [de Wijs *et al.*, 1998]. Laio *et al.*, [2000] combined first-principles total energy and force calculations for a limited number of time steps with a semi-empirical potential fit to the first-principle results.

### Elastic Constants

Seismic wave propagation is governed by the elastic constants, and the density. In most cases, seismic frequencies are sufficiently high that the adiabatic elastic constants,  $c_{ijkl}^S$ , are relevant. First-principles calculations of the type described here yield the isothermal elastic constants,  $c_{ijkl}^T$ , most directly, and a conversion must be applied [Davies, 1974]

$$c_{ijkl}^S = c_{ijkl}^T + \frac{T}{\rho C_V} \lambda_{ij} \lambda_{kl}, \quad (10)$$

where  $C_V$  is the specific heat at constant volume and

$$\lambda_{ij} = \sum_{l, k \leq l} \alpha_{kl} c_{ijkl}^T. \quad (11)$$

The thermal expansivity tensor  $\alpha_{ij}$  for a hexagonal system has only entries in the diagonal with

$$\alpha_{11} = \alpha_{22} = 1/a \cdot (\partial a / \partial T)_P, \quad \alpha_{33} = 1/c \cdot (\partial c / \partial T)_P, \quad (12)$$

the linear thermal expansivity of the  $a$ - and  $c$ -axis, respectively.

Under conditions of isotropic pre-stress, elastic wave propagation is governed by the so-called stress-strain coefficients which are defined by

$$\sigma_{ij} = c_{ijkl}^T \varepsilon_{kl}, \quad (13)$$

with  $\sigma_{ij}$  the stress and  $\varepsilon_{ij}$  the strain. Other definitions of the elastic constants have appeared in the literature [Barron and Klein, 1965]: one may define elastic constants as the second strain derivatives of the free energy,

which are not equivalent to (13) in general. If the pre-stress is isotropic, and if the applied strain is isochoric to all orders, then the free energy may be directly related to the stress-strain coefficients

$$F(V, \varepsilon'_{ij}, T) = F(V, 0, T) + \frac{1}{2} c'_{ijkl}(V, T) \varepsilon'_{ij} \varepsilon'_{kl}. \quad (14)$$

where the primes indicate the deviatoric strain. This relationship has been used to calculate the elastic constants from first-principles calculations of the total energy alone [Cohen *et al.*, 1997; Steinle-Neumann *et al.*, 1999]. The elastic constants may also be calculated by appealing to the dissipation-fluctuation theorem which relates the  $c'_{ijkl}$  to fluctuations in the shape of the crystal at constant stress. This provides one means of calculating the elastic constants in molecular dynamics simulations [Parrinello and Rahman, 1982; Wentzcovitch, 1991].

Elastic wave velocities are related to the elastic constants by the Christoffel equations

$$(c'_{ijkl} n_j n_k - \rho v^2 \delta_{il}) u_i = 0, \quad (15)$$

where  $\vec{n}$  is the propagation direction and  $\vec{u}$  the polarization of the wave,  $v$  the phase velocity, and  $\delta_{il}$  is the Kronecker delta function. Solving (15) for a given propagation direction yields three velocities, one with quasi-longitudinal polarization ( $v_P$ ), and two with quasi-transverse polarizations ( $v_S$ ). From the full elastic constant tensor, we may also determine the bulk ( $K_S$ ) and shear ( $G$ ) moduli using Hashin-Shtrikman bounds [Watt and Peselnick, 1980] which give tighter bounds on  $G$  than the usually used Voigt-Reuss-Hill averages [Hill, 1963]. The isotropically averaged aggregate velocities  $v_P$  and  $v_S$  can then be calculated by

$$v_P = \sqrt{\frac{K_S + \frac{4}{3}G}{\rho}}, \quad v_S = \sqrt{\frac{G}{\rho}} \quad (16)$$

Usually the Voigt notation is used to represent elastic constants, replacing the fourth rank tensor  $c_{ijkl}$  with a  $6 \times 6$  pseudomatrix in which pairs of indices are replaced by a single index utilizing the symmetry of the stress and strain tensors:

$$\begin{aligned} 11 \rightarrow 1; & \quad 22 \rightarrow 2; & \quad 33 \rightarrow 3; & \quad (17) \\ 23, 32 \rightarrow 4; & \quad 13, 31 \rightarrow 5; & \quad 12, 21 \rightarrow 6. \end{aligned}$$

In this notation the five single crystal elastic constants for a hexagonal system are: the longitudinal elastic constants  $c_{11}$  and  $c_{33}$ , the off-diagonal elastic constants,  $c_{12}$  and  $c_{13}$ , and a shear constant  $c_{44}$ . In the following discussions we also refer to another linearly dependent shear constant for comparison with  $c_{44}$ :  $c_{66} = 1/2(c_{11} - c_{12})$ . To calculate the five elastic constants with a first-principles total energy method, we must evaluate the effect of five different strains on the free energy (14). The bulk modulus and the change in the equilibrium  $c/a$

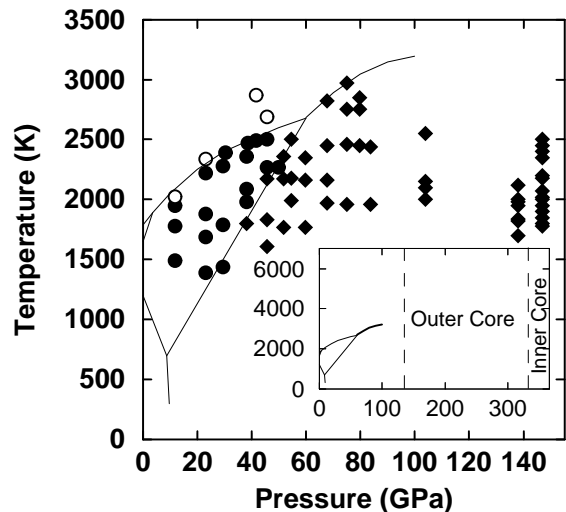


FIG. 3: Phase diagram of iron from diamond anvil cell experiments. Stable crystalline phases are bcc at ambient conditions, fcc (solid circles) at high temperature, and hcp (diamonds). Liquid iron is shown in the open symbols. bcc also has a small phase stability field at low pressure immediately below melting. Data are from Shen *et al.* [1998] and Shen and Heinz [1998]. The inset shows the pressure-temperature range relevant for a study of the inner core.

ratio with compression provide two pieces of information, yielding two independent combinations of elastic constants. The application of three isochoric strains, of hexagonal, orthorhombic, and monoclinic symmetry, yield the other three pieces of information necessary to obtain the full elastic constant tensor [Steinle-Neumann *et al.*, 1999].

## PHYSICAL PROPERTIES OF DENSE IRON

### Phase Diagram

To the extent that the inner core is composed of pure iron (or nearly pure iron), the phase diagram of iron determines the crystalline structure of the inner core. Despite considerable progress in experimental determination of the phase diagram and melting at pressures approaching those of the core, the stable phase of iron at inner core conditions can not yet uniquely be identified.

This issue is of great geophysical and geochemical importance. First, it is central in our understanding of inner core anisotropy. Different phases of iron show a distinctly different single crystal anisotropy both in magnitude and symmetry [Stixrude and Cohen, 1995b]. The enthalpy of various phases and hence the amount of latent heat released at the inner core boundary may depend strongly on the crystalline phase. Finally, the ability to incorporate impurities may be determined by the structure.

Three phases of iron have been unambiguously identified (Fig. 3): the ambient condition ferromagnetic body center cubic phase (bcc,  $\alpha$ ) is stable to about 13 GPa and up to 1200 K; at higher temperature the cubic close packed (fcc,  $\gamma$ ) phase exists, with bcc reappearing in a narrow stability field ( $\delta$ ) just below melting. The magnetic ground state of the fcc phase is a complex spin density wave [Tsunoda *et al.*, 1993; Uhl *et al.*, 1994]; in the stability field of fcc iron the local moments appear not to be ordered, however. The hexagonal close packed (hcp,  $\epsilon$ ) phase is the high pressure phase, stable to at least 300 GPa at room temperature [Mao *et al.*, 1990]. Theory predicts this phase to be non-magnetic (Pauli paramagnet) at core pressures [Söderlind *et al.*, 1996; Steinle-Neumann *et al.*, 1999]. Magnetism is not observed experimentally in the hcp phase [Taylor *et al.*, 1991], but magnetic moments on the atoms are predicted on the basis of first-principles theory [Steinle-Neumann *et al.*, 1999] up to 50 GPa. Moreover, magnetism is observed in epitaxially grown overexpanded lattices of hcp iron [Maurer *et al.*, 1991], consistent with theoretical predictions. The possible presence of magnetic states in hcp iron is important for understanding the equation of state (see below) and the phase diagram in the sub-megabar range. The competition between magnetic and non-magnetic contributions to the internal energy, differences in vibrational and magnetic entropy, and differences in volume all contribute to phase stability in iron [Moroni *et al.*, 1996].

Two experimental lines of evidence suggest additional stable polymorphs of iron at high pressure and temperature. First, in the shock wave experiment by Brown and McQueen [1986] (see also Brown *et al.* [2000] and Brown [2001]) there are two discontinuities in  $v_P$ , one at 200 GPa, the other 243 GPa (Fig. 4).

While the one at higher pressure was associated with melting of the sample, the lower one was originally attributed to the hcp to fcc phase transition. With a better characterization of the phase diagram at lower temperature and pressure today this is an unlikely scenario: the fcc-hcp phase transition ends with a triple point at much lower pressure (Fig. 3) [Shen *et al.*, 1998; Boehler, 2000]. Re-appearance of the bcc phase of iron has been suggested as an explanation of the apparent solid-solid phase transformation at 200 GPa [Matsui and Anderson, 1997]. However, first-principles theory shows that the bcc phase is mechanically unstable at high pressure and is unlikely to exist as a stable phase [Stixrude and Cohen, 1995a; Söderlind *et al.*, 1996; Vočadlo *et al.*, 2000]. An alternative interpretation attributes the first discontinuity to the onset of melting, with melting completed only at 243 GPa [Boehler and Ross, 1997]. A recent repetition of the experiment of Brown and McQueen [1986] has been unable to resolve whether or not a phase transformation in addition to melting occurs on the Hugoniot [Nguyen and Holmes, 2001].

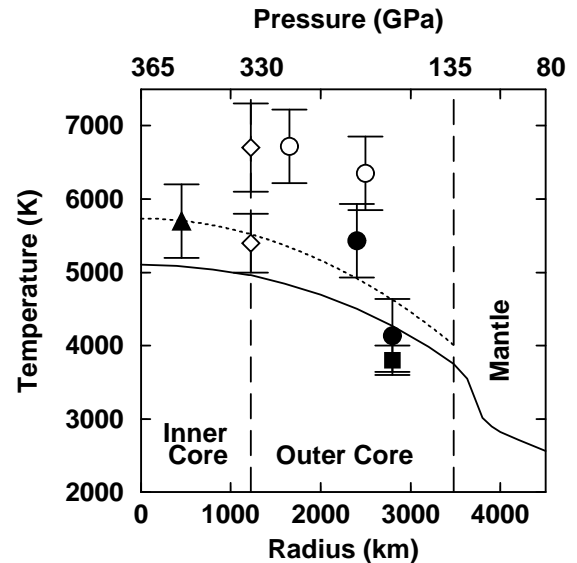


FIG. 4: Melting temperatures of iron and estimates of the geotherm in Earth’s core, with the geotherm from Stacey [1992] in the solid line. Experiments on melting of iron are shown with a square from static diamond anvil cell experiments [Boehler, 1993] and with circles for melting along the Hugoniot (solid from Brown and McQueen [1986] and open from Yoo *et al.* [1993]). The two points from Brown and McQueen [1986] show the uncertainty in the detection of melting: both points represent discontinuities in acoustic velocity along the Hugoniot, and the occurrence of melting is ambiguous. Two points from Yoo *et al.* [1993] bracket melting as observed with optical pyrometry. Diamonds show theoretical estimates of the melting point of iron at the pressure of the inner core boundary by Alfè *et al.* [1999] (upper symbol) and Laio *et al.* [2000] (lower symbol). Inner core temperature estimated from a comparison of inner core elasticity with that of iron [Steinle-Neumann *et al.*, 2001] is shown with a solid triangle. The dashed line is an adiabat through the core, based on the latter result.

Second, additional phases of iron have been proposed on the basis of static high-pressure experiments. X-ray diffraction patterns measured in laser heated diamond anvil cell experiments have been argued to be incompatible with any known iron polymorph [Saxena *et al.*, 1995; Yoo *et al.*, 1995; Andrault *et al.*, 1997]. The anomalous signal is subtle, and the proposed structures, a double hexagonal dhcp [Saxena *et al.*, 1995; Yoo *et al.*, 1995] and an orthorhombic structure [Andrault *et al.*, 1997], are closely related to hcp. Using in-situ X-ray diffraction Shen *et al.* [1998] found only fcc and hcp phases at pressure and temperature, while the dhcp phase was observed in temperature quenched samples. Andrault *et al.* [1997] used high strength pressure media which could induce non-hydrostatic conditions [Boehler, 2000]. Vočadlo *et al.* [2000] examined the relative stability of proposed high pressure phases using computational *ab-initio* methods, and found that the orthorhombic structure is mechani-

cally unstable, and that the dhcp phase is energetically less favored than hcp.

Most measurements of the melting temperature of iron from static experiments show reasonable agreement up to a pressure of 100 GPa, where the melting point is 2800-3300 K [Shen and Heinz, 1998; Boehler, 2000; Hemley and Mao, 2001]; the data of Williams *et al.* [1987] yield a significantly higher temperature at 100 GPa (4100 K). The highest pressure datum from diamond anvil cell experiments is at 200 GPa where Boehler [1993] finds the melting point at 3800 K (Fig. 4).

As mentioned above, in shock wave experiments the temperature is not determined directly; based on their dynamic compression data Brown and McQueen [1986] calculated the temperature at the Hugoniot melting point (243 GPa) to be in the range of 5000 to 5700 K (Fig. 4), consistent with subsequent theoretical calculations of the Hugoniot temperature [Wasserman *et al.*, 1996]. Measurements of the temperature by optical pyrometry yield a melting point between 235 and 300 GPa with temperatures of 6350 and 6720 K, respectively [Yoo *et al.*, 1993].

Two *ab-initio* calculations of the melting curve of iron have been carried out, yielding inconsistent results (Fig. 4). Alfè *et al.* [1999] found a melting temperature of  $6700 \pm 600$  K at the inner core boundary by comparing Gibbs free energies of solid and liquid. Laio *et al.* [2000] determined a considerably lower temperature of  $5400 \pm 400$  K. The origin of these discrepancies are not clear, but may be related to the quality of the anharmonic corrections in the study of Alfè *et al.* [1999], the semi-empirical potential used to augment first-principles calculations in the study of Laio *et al.* [2000], or different statistical sampling and runtime adopted in these two studies. In this context, it is worth pointing out that theoretical calculations of the melting temperature are extremely demanding as they involve the comparison of two large numbers (Gibbs free energies of solid and liquid) which must both be calculated to high precision.

### Static Equation of State

Experimental measurements and theoretical predictions of the equation of state of non-magnetic hcp iron agree well at core pressures (Fig. 5). At relatively low pressures, however, a discrepancy develops that is larger than that for the bcc phase and what is typical for other transition metals [Körling and Hähgglund, 1992; Steinle-Neumann *et al.*, 1999] suggesting that fundamental aspects of the physics of hcp iron may not be well understood to date.

Although experiment has so far not detected magnetism in hcp iron, recent first-principles theoretical calculations have found stable magnetic states [Steinle-Neumann *et al.*, 1999]. These are more stable than the non-magnetic state by more than 10 mRy at low pres-

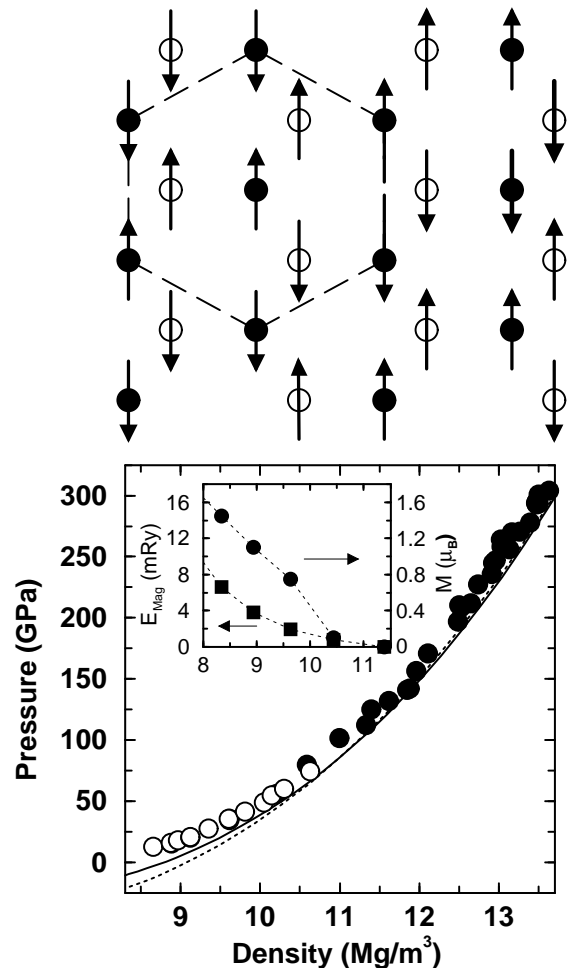


FIG. 5: Equation of state for hcp iron in the lower panel. Static theoretical results are compared to room temperature diamond anvil cell experiments by Jephcoat *et al.* [1986] (open circles) and Mao *et al.* [1990] (solid circles). The dashed line shows non-magnetic results [Stixrude *et al.*, 1994], the solid line the density-pressure relation for an antiferromagnetic structure (afmII) [Steinle-Neumann *et al.*, 1999]. The inset shows the magnetic moment (circles) and associated magnetic stabilization energy (squares) for the afmII structure. The afmII structure itself with atoms at  $z=1/4$  in solid,  $z=3/4$  in open circles is displayed in the upper panel. Arrows indicate the spin polarization of the atoms.

sure. The most stable magnetic arrangement found so far is one of antiferromagnetic ordering (afmII, Fig. 5) which retains a finite moment up to 50 GPa, well into the pressure region where hcp iron is stable [Steinle-Neumann *et al.*, 1999]. Because magnetism tends to expand the lattice, the presence of magnetism reduces the discrepancy between experimental and theoretical equations of state considerably. It is likely that still more stable magnetic states will be found, and that the ground state is a more complex magnetic structure involving spin-glass like disorder, incommensurate spin density waves, non-collinear magnetism, or a combination of these [Cohen *et*

*al.*, 2002].

### Static Elastic Constants

A comparison shows considerable disagreement of the single crystal elastic constants (Fig. 6) between experiment [Mao *et al.*, 1998; Singh *et al.*, 1998b] and theory [Stixrude and Cohen, 1995b; Söderlind *et al.*, 1996; Cohen *et al.*, 1997; Steinle-Neumann *et al.*, 1999]. The difference in the longitudinal constants  $c_{11}$  and  $c_{33}$  decreases from  $\sim 50\%$  at low pressure to a little more than 10% at high compression. As pronounced is the discrepancy for the shear elastic constants: the difference in  $c_{44}$  increases with compression to 30%, and  $c_{66}$  differs as much as 40% at high pressure, and by a factor of two at the low density data point.

Because the full elastic constant tensor of hcp iron has been measured only by the new lattice strain technique, the large discrepancy between experiment and theoretical prediction prompted a stringent comparison of both methods for a well characterized hcp metal. For the 5d transition metal rhenium, ultrasonic measurements of elastic constants were not only performed at ambient condition, but also up to 0.5 GPa, constraining the initial pressure slope (Fig. 6) [Manghnani *et al.*, 1974]. Calculated elastic constants at zero pressure and their compression dependence [Steinle-Neumann *et al.*, 1999] show excellent agreement with the ultrasonic data. In contrast, lattice strain experiments [Duffy *et al.*, 1999] do not compare favorably with either result. One of the longitudinal elastic constants ( $c_{33}$ ) is considerably smaller (20%), and as in the case for iron the shear constant  $c_{44}$  shows the largest discrepancy, being larger than the ultrasonic value by 50%. This comparison indicates that additional factors other than elasticity influence the measurements in lattice strain experiments. Subsequently it has been found that strong lattice preferred orientation developed in the experiments for hcp iron [Wenk *et al.* 2000b; Matthies *et al.*, 2001], which may cause the assumption of stress homogeneity to be violated.

For aggregate  $v_P$  and  $v_S$ , the discrepancies between theory and experiment are smaller, but still significant (Fig. 7). Part of the discrepancy between theory and experiment may be attributed to the equation of state. Since theory overestimates the density of hcp iron at low pressure, one expects the elastic wave velocities to be overestimated. The reduction of bulk modulus for the afmII magnetic state will yield lower compressional wave velocity, but for a quantitative comparison of  $v_P$  and  $v_S$  information on the full elastic constant tensor for this orthorhombic structure (with nine independent elastic constants) will be needed. The LA phonon data ( $v_P$ ) by Fiquet *et al.* [2001] at high compression and the  $v_S$  from Anderson *et al.* [2001] at low pressure appear to be anomalous as they fall below the shock wave data [Brown

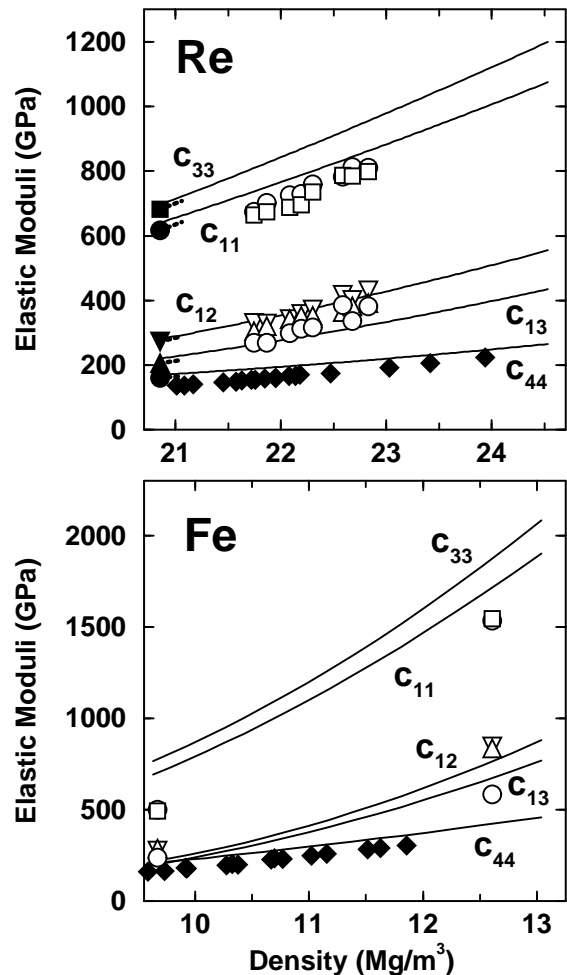


FIG. 6: Single crystal elastic constants for hcp rhenium (upper panel) and iron as a function of compression. The solid lines are Eulerian finite strain fits to computational results [Steinle-Neumann *et al.*, 1999]. Open symbols show lattice strain experiments from Duffy *et al.* [1999] for rhenium and Mao *et al.* [1998] for iron:  $c_{33}$  squares,  $c_{11}$  circles,  $c_{12}$  triangles down,  $c_{13}$  triangles up, and  $c_{44}$  circles. The shear elastic constant  $c_{44}$  as inferred from Raman frequency measurements are shown with diamonds; data for rhenium are from Olijnyk *et al.* [2001], for iron from Merkel *et al.* [2000]. For rhenium ultrasonic measurements are available at low pressure [Manghnani *et al.*, 1974] (filled symbols as above, with initial pressure dependence indicated).

and McQueen, 1986] which, due to thermal effects, would be expected to yield smaller sound velocities than room temperature experiments.

### Thermal Equation of State

The Hugoniot provides the strongest constraint on the equation of state of iron at core conditions. First-principles theoretical calculations of the Hugoniot [Wasserman *et al.*, 1996; Laio *et al.*, 2000; Alfè *et al.*, 2001]

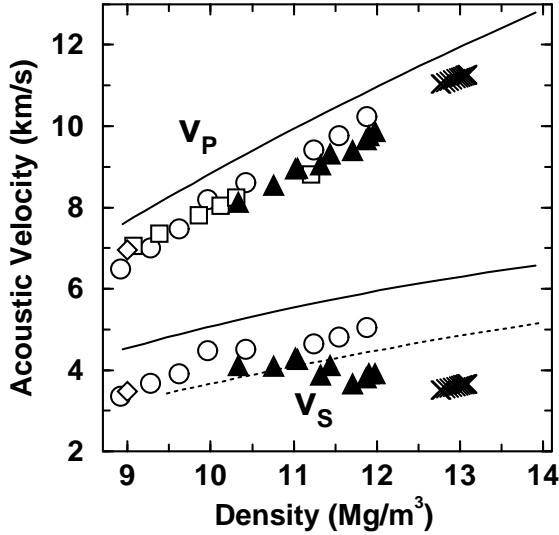


FIG. 7: Aggregate acoustic velocities for hcp iron and the inner core (crosses). Compressional ( $v_P$ ) and shear ( $v_S$ ) wave velocity are shown from first-principles calculations in solid lines for the non-magnetic state [132]. Experimental results at ambient temperature are based on the phonon density of states (open circles) [Mao *et al.*, 2001], the longitudinal acoustic phonon frequency (open squares) [Fiquet *et al.*, 2001], ultrasonic measurements (open diamonds) [Mao *et al.*, 1998], and the intensity of x-ray diffraction peaks (dashed line) [Anderson *et al.*, 2001]. For comparison shock wave experimental data in the stability field of hcp iron is included (filled triangles) [Brown and McQueen, 1986]: for the shock wave results temperature increases with compression resulting in a temperature of approximately 4500 K at the highest density point in the figure.

have typically found excellent agreement with that experimentally measured [Brown and McQueen, 1986].

A direct comparison of solid state properties between shock wave experiments and computations at inner core pressures is unfortunately not possible, as the Hugoniot is in the stability field for the liquid above 250 GPa as discussed above. We have performed a detailed comparison of the properties of iron at inner core conditions obtained from several first-principles theoretical calculations [Laio *et al.*, 2000; Alfè *et al.*, 2001; Steinle-Neumann *et al.*, 2001] and from static [Dubrovinsky *et al.*, 2000] and dynamic compression experiments (Fig. 8). The properties of iron determined from these sources agree with each other to within 2% in pressure and to within 10% in bulk modulus at 13 Mg/m<sup>3</sup> and 6000 K. This comparison supports the conclusion that the inner core is not pure iron, but that it must contain a small amount of lighter elements. Iron is consistently found to be denser than the inner core, even at a temperature of 7000 K. The bulk modulus of iron, while showing considerably more scatter, appears to be consistent with that of the inner core at a temperature near 6000 K.

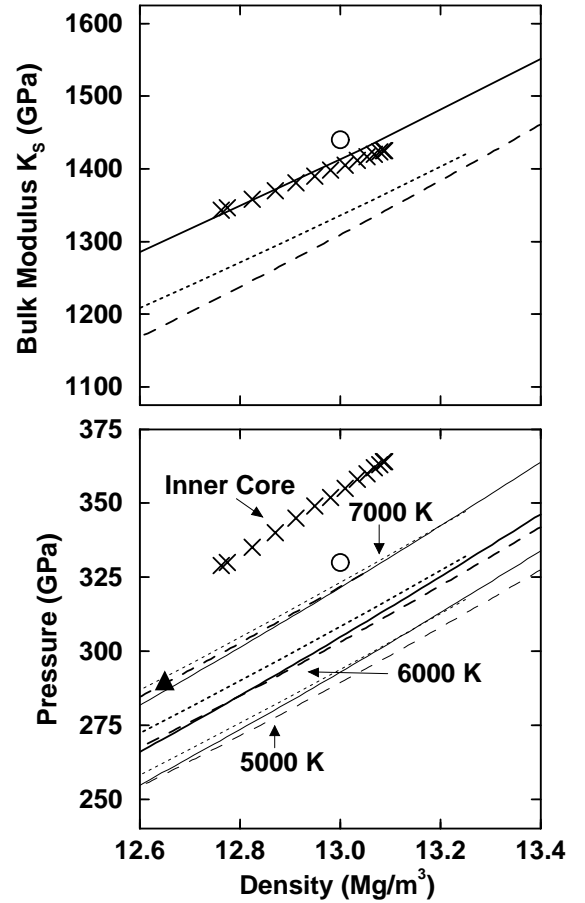


FIG. 8: Finite temperature equation of state of hcp iron. The lower panel shows a comparison for pressure-density relation in the inner core (crosses) and for hcp iron at temperatures of 5000 K, 6000 K, and 7000 K. Experimental data (long dashed lines) from Dubrovinsky *et al.* [2000] are extrapolated to inner core conditions. Two sets of calculations are from Steinle-Neumann *et al.* [2001] (solid lines) and from Alfè *et al.* [2001] (dashed lines). For comparison included are pressure and density on the Hugoniot at 7000 K (triangle) [Brown and McQueen, 1986], and results by Laio *et al.* [2000] at 5400 K (open circles). The upper panel compares the corresponding adiabatic bulk moduli along 6000 K isotherms with those of the inner core (same symbols). For the theoretical results by Alfè *et al.* [2001] and Steinle-Neumann *et al.* [2001]  $K_S$  is calculated self-consistently.  $K_T$  from static experiments [Dubrovinsky *et al.*, 2000] and the result from Laio *et al.* [2000] are converted using thermodynamic parameters from theory.

### Structure

The axial ratio  $c/a$  of the hexagonal unit cell is important for understanding the elastic anisotropy. Among transition metals at ambient conditions, the value of  $c/a$  is found to be correlated with the longitudinal wave anisotropy, which can be characterized by the ratio  $c_{33}/c_{11}$ . Large values of  $c/a$  are associated with a rel-

atively small  $c_{33}$  and slow P-wave propagation along the  $c$ -axis [Simmons and Wang, 1971]. A change in axial ratio through compression or temperature could change the single crystal anisotropy considerably.

Similar to most ambient condition hcp transition metals iron crystallizes with an axial ratio  $c/a$  slightly below the ideal value ( $\sim 1.6$ ) [Jephcoat et al., 1986; Stirrude et al., 1994]. It changes little with compression, experiments show a slight decrease with pressure, theory a minor increase.

At ambient pressure, hcp transition metals typically show significant but small changes in  $c/a$  up to high homologous temperature [Eckertlin and Kandler, 1971]. The ratio  $c_{33}/c_{11}$  shows correspondingly small changes [Simmons and Wang, 1971]. The largest change in this ratio is exhibited by titanium which shows a change of 13%. Experiments on hcp iron at higher pressure observed a small increase in  $c/a$  with temperature in the pressure range of 15-30 GPa and temperatures up to 1200 K (Fig. 9) [Huang et al., 1987; Funamori et al., 1996; Uchida et al., 2001]. Similarly, Dubrovinsky et al. [1999] report a  $c/a=1.623$  at 61 GPa and 1550 K. However, these results can be questioned on the grounds that non-hydrostatic stress may have influenced the temperature dependence of  $c/a$ , a contention supported by hysteresis on a heating and cooling cycle seen in the data of Funamori et al. [1996], and data by Dubrovinsky et al. [2000] at 185 GPa and 1115 K with a small  $c/a$  (1.585).

First-principles theoretical calculations have predicted a significant temperature induced increase in the  $c/a$  ratio of hcp iron [Wasserman et al., 1996; Steinle-Neumann et al., 2001], which is apparently consistent with the majority of the existing experimental data. For an inner core density of  $13.04 \text{ Mg/m}^3$  the axial ratio increases from the static value close to 1.6 to about 1.7 at 6000 K (Fig. 10). This implies that at constant density the  $c$ -axis grows at the expense of the  $a$ -axis. The linear thermal expansivities  $\alpha_{11}$  and  $\alpha_{33}$  at constant pressure provide another way to represent the change in structural properties. Over a wide range of thermodynamic conditions, the  $a$ -axis is predicted to compress slightly with increasing temperature (Fig. 11).

The temperature-induced change in  $c/a$  appears to depend on the absolute temperature rather than homologous temperature: the reason that  $c/a$  of hcp iron reaches such large values at inner core conditions appears to be that higher sub-solidus temperatures may be reached. The origin of the temperature induced increase in  $c/a$  can be traced to the vibrational entropy, other contributions to the vibrational and electronic free energy have little effect (Fig. 12). Our calculations show that the entropy increases substantially with increasing  $c/a$ . The entropic contribution to the free energy depends on the absolute temperature

$$F_{vib} = E_{vib} - TS_{vib} \quad (18)$$

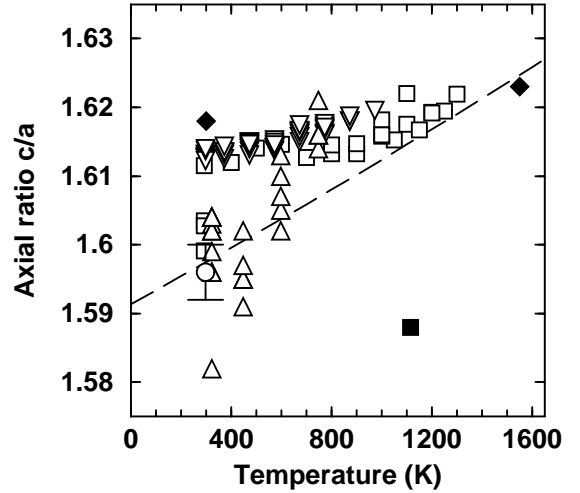


FIG. 9: Axial ratio  $c/a$  of hcp iron as a function of temperature. The dashed line shows theoretical results for a density of  $12.52 \text{ Mg/m}^3$  corresponding to a static pressure of 195 GPa [Steinle-Neumann et al., 2001]. The symbols show a polybaric set of experimental data at lower pressures, with measurements in the pressure range of 15-20 GPa from Uchida et al. [2001] (triangles down) and Huang et al. [1987] (triangles up). Open squares from Funamori et al. [1996] are in the pressure range of 23-35 GPa. Higher pressure data are from Dubrovinsky et al. [1999] (61 GPa, filled diamonds) and Dubrovinsky et al. [2000] (185 GPa, square). For comparison the room temperature axial ratio from Mao et al. [1990] (197 GPa, open circle) is included. The experimental uncertainty shown for Mao et al. [1990] can be taken as representative.

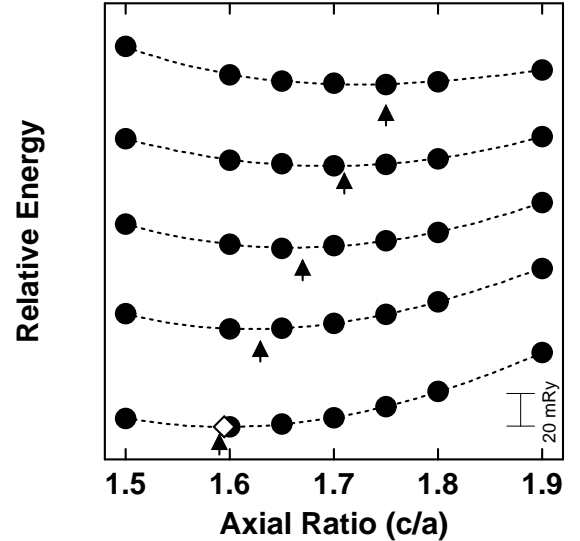


FIG. 10: Relative energies ( $F$ ) for hcp iron at an inner core density of  $13.04 \text{ Mg/m}^3$  as a function of axial ratio  $c/a$  for temperature increments of 2000 K, starting with the static results at the bottom [Steinle-Neumann et al., 2001]. Arrows indicate the minima on the lines, showing significant increase in equilibrium  $c/a$  with temperature. The open diamond is the experimentally determined  $c/a$  at room temperature and 270 GPa [Mao et al., 1990].

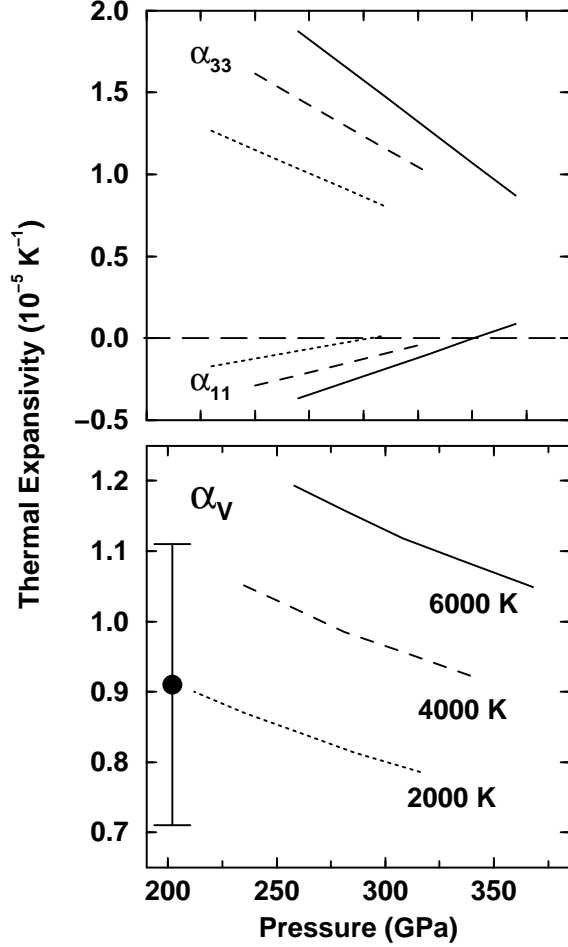


FIG. 11: Thermal expansivity of iron at high pressure. The lower panel shows the volume thermal expansivity  $\alpha_V$  of hcp iron at temperatures of 2000 K, 4000 K, and 6000 K. The experimental datum is from *Duffy and Ahrens [1993]* for an average thermal expansivity over the range of 300-5200 K. The upper panel shows the corresponding linear thermal expansivities for the  $a$ - ( $\alpha_{11}$ ) and  $c$ -axes ( $\alpha_{33}$ ).

so that large values of  $c/a$  become increasingly more favorable energetically at high temperature.

### High Temperature Elasticity

As a consequence of the increase in  $c/a$  the longitudinal anisotropy changes radically with temperature,  $c_{11}$  becomes larger than  $c_{33}$  (Fig. 13), with compressional wave propagation in the basal plane being faster than along the  $c$ -axis (Fig. 14). As the  $c$ -axis expands it becomes more compressible, and the corresponding longitudinal modulus,  $c_{33}$ , softens.  $c_{11}$  in turn increases slightly. The off-diagonal elastic constants are also affected by the temperature-induced change in structure:  $c_{12}$  increases rapidly with temperature because the basal plane shrinks

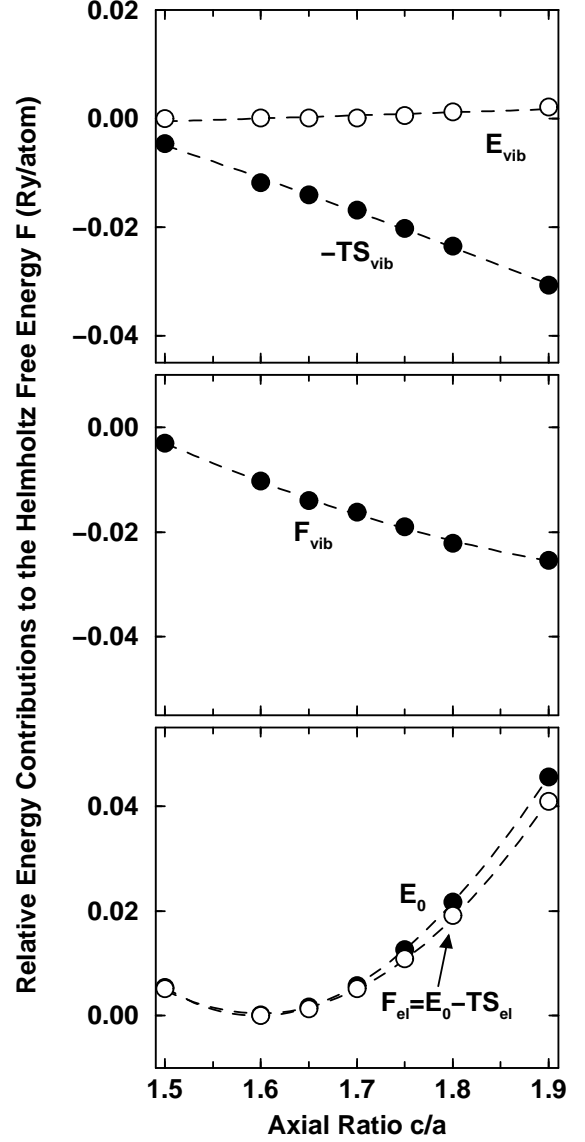


FIG. 12: Energy contributions to the total Helmholtz free energy  $F$  as a function of axial ratio for  $\rho=13.04 \text{ Mg/m}^3$  and  $T=4000 \text{ K}$ . The lower panel shows the static energy  $E$  (filled symbols) and the electronic free energy  $F_{el}$  (opaque symbols). The middle panel shows the vibrational free energy  $F_{vib}$  which is divided into internal vibrational energy  $E_{vib}$  (open symbols) and a vibrational entropy term  $-TS_{vib}$  (filled symbols) in the upper panel.

with increasing temperature at constant density.

The shear constants  $c_{44}$  and  $c_{66}$  show a strong temperature dependence and decrease almost by a factor of four at 6000 K and change order as well (Fig. 13). The velocity of shear waves is considerably smaller at high temperature and the sense of shear anisotropy is reversed (Fig. 14), with the propagation of the (001) polarized shear wave becoming faster along the  $c$ -axis than in the basal plane.

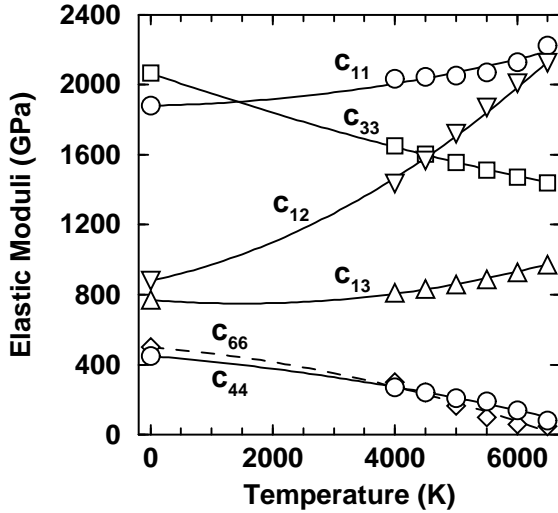


FIG. 13: Single crystal elastic constants of hcp iron at a density of  $13.04 \text{ Mg/m}^3$  [Steinle-Neumann *et al.*, 2001]. Static values are connected to high temperature results with a quadratic fit (lines): the longitudinal elastic constants  $c_{11}$  and  $c_{33}$  are shown with circles and squares, the off-diagonal constants  $c_{12}$  and  $c_{13}$  with triangles down and up, for the shear elastic constant  $c_{44}$  and  $c_{66}$  circles and diamonds are used.  $c_{66} = 1/2(c_{11} - c_{12})$  (dashed line) is not an independent elastic constant but included for comparison with  $c_{44}$ .

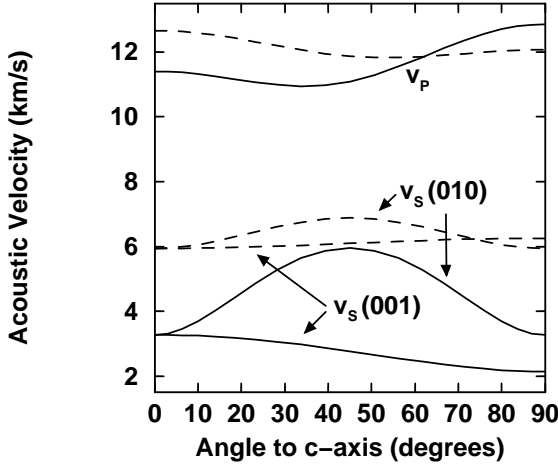


FIG. 14: Single crystal anisotropy in hcp iron from static calculations (dashed lines) and at 6000 K (solid lines) [Steinle-Neumann *et al.*, 2001]. The wave propagation velocities for the P-wave ( $v_P$ ) and the two polarizations of the S-wave ( $v_S$ , with polarizations given in the parentheses) are shown as a function of the angle with respect to the  $c$ -axis.

Our calculations imply a shear instability in hcp iron at very high temperature,  $c_{66}$  approaches zero at 7000 K yielding an upper bound on its mechanical stability or melting point. This is in qualitative agreement with the results by Laio *et al.* [2000] who predict a shear instability at somewhat lower temperature.

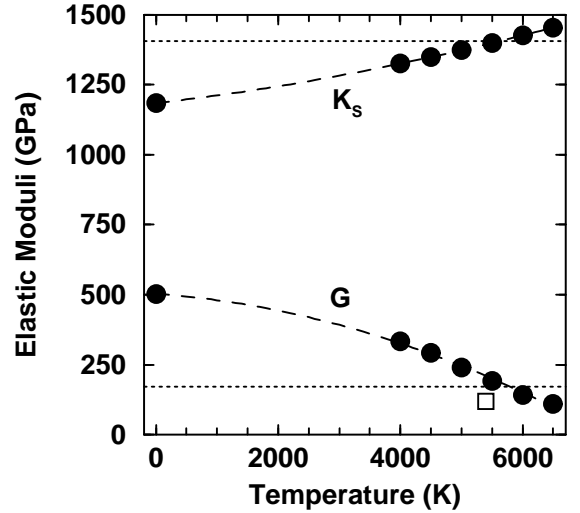


FIG. 15: Aggregate acoustic properties of iron calculated as a function of temperature [Steinle-Neumann *et al.*, 2001] in comparison to the inner core. The adiabatic bulk ( $K_S$ ) and shear moduli ( $G$ ) at  $13.04 \text{ Mg/m}^3$  are shown as a function of temperature (solid circles) with the corresponding values of the inner core at the same density (dotted lines). The open square shows a previous computational result by Laio *et al.* [2000].

## PROPERTIES OF THE INNER CORE

### Aggregate Elasticity

Our current understanding of the physical properties of iron shows that the high Poisson's ratio of the inner core can be explained by solid-phase elasticity [Laio *et al.*, 2000; Steinle-Neumann *et al.*, 2001]. The shear elastic constants are predicted to decrease rapidly with increasing temperature - by a factor of four at 6000 K. As a result,  $G$  becomes rapidly smaller with increasing temperature (Fig. 15), leading to a Poisson's ratio of hcp iron that is in quantitative agreement with seismic models of the inner core. These results confirm inferences on the basis of shock wave measurements of  $v_P$  and estimates of  $v_S$  at core conditions [Brown and McQueen, 1986]. It does not seem necessary to invoke additional mechanisms to explain the high Poisson's ratio of the inner core such as viscoelastic dispersion [Jackson *et al.*, 2000] or the presence of partial melt [Singh *et al.*, 2000].

### Temperature

Knowledge of the elasticity of iron permits an estimate of inner core temperature that is independent of the iron melting curve and the associated uncertainties related to freezing point depression. The temperature of the inner core is estimated to be  $5700 (\pm 500) \text{ K}$ . At this temper-

ature Poisson's ratio,  $K_S$ , and  $G$  of iron simultaneously agree with the properties of seismological models of the inner core (Fig. 15). We infer that the additional light elements that must be present in the inner core have a greater effect on the density through a decrease in mean atomic weight, than they do on the elastic moduli. Further investigations of the elasticity of iron-light element alloys will be needed to test this hypothesis.

Based on an estimate of the Earth's central temperature, we may construct a core geotherm. We assume that the temperature distribution in the inner and outer core are adiabatic and adopt  $\gamma = 1.6$  [Wasserman *et al.*, 1996; Alfè *et al.*, 2001] for the inner core, and  $\gamma = 1.5$  for the outer core (Fig. 4). The latter value is consistent with shock wave data [Brown and McQueen, 1986]. With this choice the temperature is 5750 K in the center of the Earth, 5500 K at the inner core boundary, and 4000 K at the core mantle boundary (Fig. 4).

Other estimates of the temperature at the inner core boundary fall in the range of 4500-6000 K, depending on melting point estimate and degree of melting point depression. Our temperature is somewhat higher than the geotherm given by Brown and McQueen [1986] with 5000 K at the inner core boundary, and also higher than the extrapolation from static experiments ( $< 5000$  K) [Boehler, 2000] or that based on the melting point from Laio *et al.* [2000] (5400 K). The melting point from Alfè *et al.* [1999], which is similar to that measured by Yoo *et al.* [1993], combined with an assumed melting point depression of 700 K [Alfè *et al.*, 2002] yields a inner core boundary temperature at 6000 K.

### Simplified Model of Texture and Anisotropy

The sense of anisotropy that is found at high temperature changes our view of the polycrystalline texture of the inner core and the dynamic processes that may produce it. On the basis of first-principles calculations of the elastic constants, we propose a simple model of the polycrystalline texture of the inner core that explains the main features of its anisotropy [Steinle-Neumann *et al.*, 2001]. We find that if 1/3 of the basal planes are aligned with Earth's rotation axis in an otherwise randomly oriented medium, compressional wave travel time anomalies are well explained (Fig. 16). This model is almost certainly over-simplified. The key element is the tendency for the fast crystallographic direction ( $a$ ) to be aligned with the observed symmetry axis of inner-core anisotropy (approximately polar). It is probable that the actual direction and degree of crystallographic alignment will vary with geographic location. Such variations may account for seismological observations of heterogeneity [Creager, 1997; Tanaka and Hamaguchi, 1997; Vidale and Earle., 2000].

Important remaining questions include the origin of

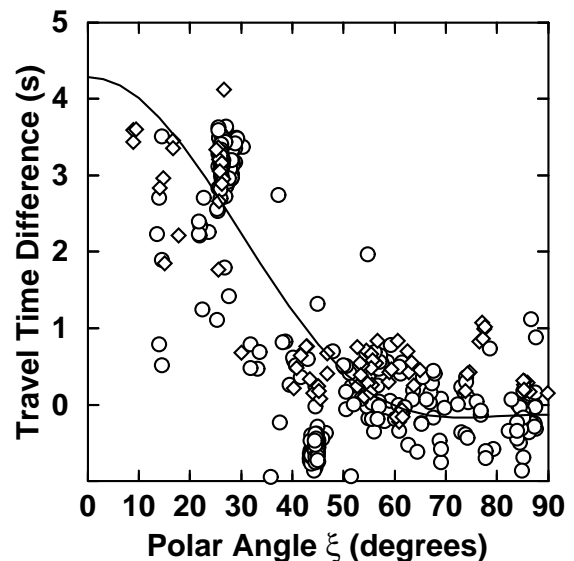


FIG. 16: Differential travel time differences of PKIKP-PKP (BC-DF) due to inner core anisotropy as a function of propagation direction. The solid line shows the results based on a model of the inner core in which 1/3 of the crystals have their basal planes aligned with the rotation axis in conjunction with the high temperature elastic constants for hcp iron from Steinle-Neumann *et al.* [2001]. Seismological observations are from Song and Helmberger [1993] (diamonds) and Creager [1999; 2000] (circles).

polycrystalline texture in the inner core, which may have been acquired during solidification, or may have developed subsequently as a result of plastic deformation, as discussed above. If plastic deformation is the prevalent texturing mechanism as we have argued, crystal alignment must depend on the dominant microscopic deformation mechanism in hcp iron at inner core conditions or patterns of growth and recrystallization, and the source of the stress field. While these are currently unknown, our simple model is consistent with the available information.

Candidates for the deformation mechanism include diffusion and recrystallization [Yoshida *et al.*, 1996; Stixrude and Cohen, 1995b] dislocation glide [Wenk *et al.*, 1988; Wenk *et al.*, 2000b; Poirier and Price, 1999], or a combination of both [Buffett and Wenk, 2001]. The type of deformation mechanism is determined by the magnitude of stress and the grain size of the material. When stresses are large, dislocation creep dominates because a large dislocation density facilitates the slip along crystal planes; if the stress is small with a low dislocation density diffusion creep prevails as diffusion of point defects dominates deformation. Small grains facilitate diffusion, larger grain sizes favor dislocation glide. Estimates on the grain size of the crystals in the inner core range from a few mm [Buffett, 1996] to the km scale [Bergman, 1998]. With the critical grain size determining

the deformation regime being in the meter range [Yoshida *et al.*, 1996] the large uncertainty in grain size does not provide the means to favor one over the other.

Yoshida *et al.* [1996] argue that diffusion and recrystallization would result in a texture with the elastically stiffest (fastest) axis coinciding with the direction of the flow, minimizing the strain energy; for iron at high temperature this would tend to align basal planes with the dominant pattern of flow. Among the crystallographic slip planes that may participate in dislocation glide, the basal plane is the slip system that is most easily activated at high pressure according to recent theoretical and experimental work [Poirier and Price, 1999; Wenk *et al.*, 2000b]. The predicted high axial ratio at inner core conditions would probably further enhance basal slip as it is typical for ambient hcp metals with large  $c/a$ . As crystals deform in an external stress field basal planes would rotate in the direction of maximum shear, yielding a texture with basal planes aligned with the direction of flow as well. Active recrystallization during slip would tend to enhance the resulting fabric.

Above we have discussed possible sources for stress in the inner core, which allyield distinct flow patterns. Many of them share a flow that is dominant in the polar direction [Yoshida *et al.*, 1996; Karato, 1999] which would yield a texture of basal planes aligned with Earth's rotation axis. The shear flow invoked by Buffett and Bloxham [2000] also yields a texture with the general characteristics of basal planes aligned with the polar direction [Buffett and Wenk, 2001].

To obtain the seismic characteristics of such a textural model from single crystal results we convert the elastic anisotropy of iron to differential travel time anomalies. We start by considering an aggregate in which all  $a$ -axes of hcp iron are aligned with the polar axis of the inner core but otherwise randomly oriented. We obtain the elastic properties of this aggregate by averaging elasticity over the solid angle about the  $a$ -axis [Stixrude, 1998] which again yields an aggregate elasticity of hexagonal (cylindrical) symmetry. Using the Christoffel equations (15) we can calculate  $v_P$  as function of the angle  $\xi$  between the P-wave propagation direction and the pole. Defining the amplitude of the anisotropy as

$$\delta v_P(\xi)/v_{P,av} = (v_P(\xi) - v_{P,av})/v_{P,av} \quad (19)$$

( $v_{P,av}$  is the average  $v_P$ ) we obtain an amplitude of 10% at  $\xi = 0^\circ$ . This is about a factor of three to five larger than global seismic anisotropy models for the inner core [Song, 1997; Ishii *et al.*, 2002a]. It is unlikely that crystallographic alignment in the inner core is perfect. Consequently, in our simple model, the degree of alignment is reduced by a factor of three in order to match the gross amplitude of the seismically observed anisotropy.

To compare directly with seismic observations we compute differential PKIKP travel time anomalies due to in-

ner core anisotropy by

$$\delta t(\Delta, \xi) = -t(\Delta)\delta v_P(\xi)/v_{P,av}, \quad (20)$$

where  $\Delta$  is the angular distance from source to receiver, and  $t$  the travel time of the PKIKP phase through the inner core. PKIKP and PKP<sub>BC</sub> are seen together over a narrow range of distances near  $\Delta = 150^\circ$  ( $t=124$  s) which we use as a reference distance [Stixrude and Cohen, 1995b]. The resulting differential travel time differences are in good agreement both in amplitude and angular dependence with seismic data (Fig. 16).

While we refer to plastic deformation explicitly in the development of this textural model, it is also consistent with other classes of structure. The general character of solidification texture from dendritic growth for pure zinc (like iron at high temperature, a transition metal with high  $c/a$ ) [Bergman *et al.*, 2000] is in agreement with the model we propose.

## CONCLUSIONS AND OUTLOOK

The seismically observed complexity in inner core structure and importance of inner core crystallization for geodynamo processes have initiated considerable interest in the physical state and dynamics of this innermost portion of our planet. Advances in experimental and theoretical methods in mineral physics have made it possible to address important questions regarding core composition, temperature, crystalline structure, and elasticity in the inner core.

Combining geophysical information on core structure and chemical constraints for the partitioning of elements between the solid and liquid promising steps have been made to characterize the light element composition in the core [Alfè *et al.*, 2000a; 2000b; 2002] with first results indicating that at least a ternary mixture is needed to satisfy all data. The effect of the light element on inner core elastic properties is expected to be minor, except for density, as evidenced by the ability of pure iron to reproduce inner core aggregate elastic properties [Laio *et al.*, 2000; Steinle-Neumann *et al.*, 2001].

Discrepancies in static properties of the high pressure phase of iron, hcp, between experimental data and theoretical predictions suggest that some aspect of the physics of this phase is not well understood to date. Theory indicates the possible presence of magnetic moments on the atoms in the hcp phase [Steinle-Neumann *et al.*, 1999]. Experimental and theoretical efforts should be targeted towards a better characterization of magnetic properties at pressures below 100 GPa. Theoretical investigation should focus on the characterization of more complex magnetic structures including non-collinear, disordered, and incommensurate states [Cohen *et al.*, 2002]. Also, advances in studies of phonon spectra at high pressure

will hopefully result in independent estimates of compressional and shear acoustic wave velocities and of the full elastic constant tensor in the near future.

The thermoelastic properties of iron appear to depend critically on the  $c/a$  ratio, especially the elastic anisotropy. A careful study of structural parameters as a function of pressure and temperature using experimental and independent theoretical methods could be used to test the predicted reversal in elastic anisotropy of hcp iron at high temperature [Steinle-Neumann *et al.*, 2001].

An extension of the melting curve from diamond anvil cell experiments to higher pressures could help to lower current uncertainties in the temperature of the Earth's core. However, present uncertainties in the melting point of iron are probably comparable to uncertainties in the freezing point depression. Further investigation of the phase stability and elastic properties of iron light element alloys will be important.

We greatly appreciate helpful communication of results and preprints from D. Alfè, B. Buffett, L. Dubrovinsky, O. Gülseren, M. Ishii, J. Nguyen, and J. Tromp. This work was supported by the National Science Foundation under grants EAR-9980553 (LS) and EAR-998002 (REC), and by DOE ASCI/ASAP subcontract B341492 to Caltech DOE W-7405-ENG-48 (REC). Computations were performed on the Cray SV1 at the Geophysical Laboratory, supported by NSF grant EAR-9975753 and by the W. M. Keck Foundation.

---

\* g.steinle-neumann@gl.ciw.edu; now at: Geophysical Laboratory, Carnegie Institution of Washington, Washington, DC 20015-1035

- [1] Ahrens, T. J., and R. Jeanloz, Pyrite shock compression, isentropic release, and composition of the Earth's core, *J. Geophys. Res.*, *92*, 10363-10375, 1987.
- [2] Alfè, D., M. J. Gillan, and G. D. Price, The melting curve of iron at the pressures of the Earth's core from *ab-initio* calculations, *Nature*, *401*, 462-464, 1999.
- [3] Alfè, D., M. J. Gillan, and G. D. Price, Constraints on the composition of the Earth's core from *ab-initio* calculations, *Nature*, *405*, 172-175, 2000a.
- [4] Alfè, D., M. J. Gillan, and G. D. Price, Thermodynamic stability of Fe/O solid solution at inner-core conditions, *Geophys. Res. Lett.*, *27*, 2417-2420, 2000b.
- [5] Alfè, D., G. D. Price, and M. J. Gillan, Thermodynamics of hexagonal close packed iron under Earth's core conditions, *Phys. Rev. B* *64*, 045123, 2001.
- [6] Alfè, D., M. J. Gillan, and G. D. Price, Composition and temperature of Earth's core constrained by combining *ab-initio* calculations and seismic data, *Earth Planet. Sci. Lett.*, *95*, 91-98, 2002.
- [7] Anderson, O. L., L. Dubrovinsky, S. K. Saxena, and T. LeBihan, Experimental vibrational Grüneisen ratio values for  $\epsilon$ -iron up to 330 GPa at 300 K, *grl* *28*, 399-402, 2001. Correction, *Geophys. Res. Lett.*, *28*, 2359, 2001.
- [8] Anderson, W. W., and T. J. Ahrens, Shock temperature and melting in iron sulfides at core pressure, *J. Geophys. Res.*, *101*, 5627-5642, 1996.
- [9] Andrault, D., G. Fiquet, M. Kunz, F. Visocekas, and D. Häusermann, The orthorhombic structure of iron: An in situ study at high-temperature and high-pressure, *Science*, *278* 831-834, 1997.
- [10] Asada, T., and K. Terakura, Cohesive properties of iron obtained by use of generalized gradient approximation, *Phys. Rev. B* *46*, 13599-13602, 1992. Correction, *Phys. Rev. B* *48*, 17649, 1993.
- [11] Aurnou, J.M., D. Brito, and P. L. Olson, Anomalous rotation of the inner core and the toroidal magnetic field, *J. Geophys. Res.*, *103*, 9721-9738, 1998.
- [12] Barron, T. H.K., and M. L. Klein, Second-order elastic constants of a solid under stress, *Proc. Phys. Soc. London*, *85*, 523-532, 1965.
- [13] Bergman, M. I., Measurements of elastic anisotropy due to solidification texturing and the implications for the Earth's inner core, *Nature*, *389*, 60-63, 1997.
- [14] Bergman, M. I., Estimates of the Earth's inner core grain size, *Geophys. Res. Lett.*, *25*, 1593-1596, 1998.
- [15] Bergman, M. I., L. Giersch, M. Hinczewski, and V. Izzo, Elastic and attenuation anisotropy in directionally solidified (hcp) zinc, and the seismic anisotropy in the Earth's inner core, *Phys. Earth Planet. Inter.*, *117*, 139-151, 2000.
- [16] Birch, F., The  $\alpha$ - $\gamma$  transformation of iron at high pressures, and the problem of Earth's magnetism, *Amer. J. Sci.*, *238*, 192-211, 1940.
- [17] Birch, F., Density and composition of mantle and core, *J. Geophys. Res.*, *69*, 4377-4388, 1964.
- [18] Boehler, R., Temperatures in the Earth's core from melting point measurements of iron at high static pressures, *Nature*, *363*, 534-536, 1993.
- [19] Boehler, R., High-pressure experiments and the phase diagram of lower mantle and core materials, *Rev. Geophys.*, *38*, 221-245, 2000.
- [20] Boehler, R., and M. Ross, Melting curve of aluminum in a diamond cell to 0.8 Mbar: implications for iron, *Earth Planet. Sci. Lett.*, *153*, 223-227, 1997.
- [21] Braginsky, S. I., Structure of the F layer and reasons for convection in the Earth's core, *Dokl. Akad. SSSR*, *149*, 1311-1314, 1963.
- [22] Bréger, L., B. Romanovicz, and H. Tkalčić, PKP(BC-DF) travel time residuals and short scale heterogeneity in the deep Earth, *Geophys. Res. Lett.*, *26*, 3169-3172, 1999.
- [23] Brown, G. C., and A. E. Mussett *The inaccessible Earth*, 276 pp., Chapman and Hall, London, 1993.
- [24] Brown, J. M., The equation of state of iron to 450 GPa: Another high pressure solid phase, *Geophys. Res. Lett.*, *28*, 4339-4342, 2001.
- [25] Brown, J. M., and R. G. McQueen, The equation of state for iron and the Earth's core, in *High-Pressure Research in Geophysics*, edited by S. Akimoto and M. H. Manghnani, pp. 611-623, Reidel, Dordrecht, 1982.
- [26] Brown, J. M., and R. G. McQueen, Phase transitions, Grüneisen parameter, and elasticity for shocked iron between 77 GPa and 400 GPa, *J. Geophys. Res.*, *91*, 7485-7494, 1986.
- [27] Brown, J. M., T. J. Ahrens, and D. L. Shampine, Hugoniot data for pyrrhotite and the Earth's core, *J. Geophys. Res.*, *89*, 6041-6048, 1984.

- [28] Brown, J. M., J. N. Fritz, and R. S. Hixson, Hugoniot data for iron, *J. Appl. Phys.*, *88* 5496-5498, 2000.
- [29] Buffett, B. A., A mechanism for decade fluctuations in the length of day, *Geophys. Res. Lett.*, *23*, 3803-3806, 1996.
- [30] Buffett, B. A., Geodynamic estimates of the viscosity of the Earth's inner core, *Nature*, *388*, 571-573, 1997.
- [31] Buffett, B. A., Dynamics of Earth's core, in *Earth's Deep Interior: Mineral Physics and Tomography from the Atomic to the Global Scale*, *Geophysical Monograph*, vol. 117, edited by S.-I. Karato et al., pp. 37-62, American Geophysical Union, Washington, DC, 2000.
- [32] Buffett, B. A., and J. Bloxham, Deformation of Earth's inner core by electromagnetic forces, *Geophys. Res. Lett.*, *24*, 4001-4004, 2000.
- [33] Buffett, B. A., and K. C. Creager, A comparison between geodetic and seismic estimates of inner core rotation, *Geophys. Res. Lett.*, *26*, 1509-1512, 1999.
- [34] Buffett, B. A., and H.-R. Wenk, Texturing of the inner core by Maxwell stresses, *Nature*, *412*, 60-63, 2001.
- [35] Buffett, B. A., H. E. Huppert, J. R. Lister, and A. W. Woods, On the thermal evolution of the Earth, *J. Geophys. Res.*, *101*, 7989-8006, 1996.
- [36] Bullen, K. E., A hypothesis on compressibility at compressions of the order a million atmospheres, *Nature*, *157*, 405, 1946.
- [37] Bullen, K. E., An index of degree of chemical inhomogeneity in the earth, *Geophys. J. R. Astron. Soc.*, *7*, 584-592, 1963.
- [38] Clement, B. M., and L. Stixrude, Inner-core anisotropy, anomalies in the time-averaged paleomagnetic field, and polarity transition paths, *Earth Planet. Sci. Lett.*, *130*, 75-85, 1995.
- [39] Cohen, R. E., and O. Gülseren, Thermal equation of state of tantalum, *Phys. Rev. B* *63*, 224101, 2001.
- [40] Cohen, R. E., L. Stixrude, and E. Wasserman, Tight-binding computations of elastic anisotropy of Fe, Xe, and Si under compression, *Phys. Rev. B* *56*, 8575-8589, 1997.
- [41] Cohen, R. E., S. Gramsch, S. Mukherjee, G. Steinle-Neumann, and L. Stixrude, Importance of magnetism in phase stability, equations of state, and elasticity, in *Proc. Int. School of Physics "Enrico Fermi"*, vol. 147, edited by R. Hemley et al., (in press), 2002.
- [42] Creager, K. C., Anisotropy of the inner core from differential travel times of the phases PKP and PKIKP, *Nature*, *356*, 309-314, 1992.
- [43] Creager, K. C., Inner core rotation rate from small-scale heterogeneity and time varying travel times, *Science*, *278*, 1284-1288, 1997.
- [44] Creager, K. C., Large-scale variations in inner core anisotropy, *J. Geophys. Res.*, *104*, 23127-23139, 1999.
- [45] Creager, K. C., Inner core anisotropy and rotation, in *Earth's Deep Interior: Mineral Physics and Tomography from the Atomic to the Global Scale*, *Geophysical Monograph*, vol. 117, edited by S.-I. Karato et al., pp. 89-115, American Geophysical Union, Washington, DC, 2000.
- [46] Davies, G. F., Effective elastic-moduli under hydrostatic stress- I. Quasi-harmonic theory, *J. Phys. Chem. Solids*, *35*, 1513-1520, 1974.
- [47] Deuss, A., J. H. Woodhouse, H. Paulsen, and J. Trampert, The observation of inner core shear waves, *Geophys. J. Int.*, *112*, 67-73, 2000.
- [48] Dubrovinsky, L. S., P. Lazor, S. K. Saxena, P. Häggkvist, H. P. Weber, T. LeBihan, and D. Häusermann, Study of laser heated iron using third generation synchrotron X-ray radiation facility with image plate at high pressure, *Phys. Chem. Minerals*, *26*, 539-545, 1999.
- [49] Dubrovinsky, L. S., S. K. Saxena, F. Tutti, S. Rekhi, and T. LeBihan, In situ X-ray study of thermal expansion and phase transition of iron at multimegabar pressure, *Phys. Rev. Lett.* *84*, 1720-1723, 2000.
- [50] Duffy, T. S., and T. J. Ahrens, Thermal-expansion of mantle and core materials at very high-pressures, *Geophys. Res. Lett.*, *20*, 1103-1106, 1993.
- [51] Duffy, T. S., G. Shen, D. L. Heinz, J. Shu, Y. Ma, H.-K. Mao, R. J. Hemley, and A. K. Singh, Lattice strains in gold and rhenium under nonhydrostatic compression to 37 GPa, *Phys. Rev. B* *60*, 15063-15073, 1999.
- [52] Dziewonski, A. M., and D. L. Anderson, Preliminary reference Earth model, *Phys. Earth Planet. Inter.*, *25*, 297-356, 1981.
- [53] Dziewonski, A. M., and F. Gilbert, Solidity of the inner core of the Earth inferred from normal mode observations, *Nature*, *234*, 465-466, 1971.
- [54] Eckerlin, P., and H. Kandler, Structure data of elements and intermetallic alloys, *Landolt-Börnstein*, Group III, Vol. 6, Springer, Berlin, 1971.
- [55] Fiquet, G., J. Badro, F. Guyot, H. Requardt, and M. Krisch, Sound velocities of iron to 110 Gigapascals, *Science*, *291*, 468-471, 2001.
- [56] Funamori, N., T. Yagi, and T. Uchida, High-pressure and high-temperature *in situ* x-ray diffraction study of iron to above 30 GPa using MA8-type apparatus, *Geophys. Res. Lett.*, *23*, 953-956, 1996.
- [57] Glatzmaier, G. A., and P. H. Roberts, A three-dimensional convective dynamo solution with rotating and finitely conducting inner core and mantle, *Phys. Earth Planet. Inter.*, *91*, 63-75, 1995.
- [58] Glatzmaier, G. A., and P. H. Roberts, Rotation and magnetism of Earth's inner core, *Science*, *274*, 1887-1891, 1996.
- [59] Gülseren, O., and R. E. Cohen, High pressure and temperature elasticity of bcc tantalum, *Phys. Rev. B* *65*, 064103, 2002.
- [60] Hemley, R. J., and H.-K. Mao, *In-situ* studies of iron under pressure: new windows on the Earth's core, *Int. Geology Rev.*, *43*, 1-30, 2001.
- [61] Hill, R., The elastic behaviour of a crystalline aggregate, *Proceedings of the Physical Society, London, A*, *65*, 349-355, 1952.
- [62] Hohenberg, P., and W. Kohn, Inhomogeneous electron gas, *Phys. Rev.*, *136*, B864-871, 1964.
- [63] Hollerbach, R., and C. A. Jones, Influence of the Earth's inner-core on geomagnetic fluctuations and reversals, *Nature*, *365*, 541-543, 1993.
- [64] Huang, E., W. A. Bassett, and P. Tao, Pressure-temperature-volume relationship for hexagonal close packed iron determined by synchrotron radiation, *J. Geophys. Res.*, *92*, 8129-8135, 1987.
- [65] Ishii, M., J. Tromp, A. M. Dziewonski, and G. Ekström, Joint inversion of normal-mode and body-wave data for inner core anisotropy: 1. Simple inner-core models and mantle heterogeneity, submitted to *J. Geophys. Res.*, (2002a).
- [66] Ishii, M., A. M. Dziewonski, J. Tromp, and G. Ekström,

- Joint inversion of normal-mode and body-wave data for inner core anisotropy: 2. Possible complexity within the inner core and mantle, submitted to *J. Geophys. Res.*, (2002b).
- [67] Ito, E., K. Morooka, O. Ujike, and T. Katsura, Reactions between molten iron and silicate melts at high pressure: implications for the chemical evolution of the Earth's core, *J. Geophys. Res.*, *100*, 5901-5910, 1995.
- [68] Jackson, I., J. D. F. Gerald, and H. Kokkonen, High-temperature viscoelastic relaxation in iron and its implication for the shear modulus and attenuation for the Earth's inner core, *J. Geophys. Res.*, *105*, 23605-23634, 2000.
- [69] Jeanloz, R., Properties of iron at high pressures and the state of the core, *J. Geophys. Res.*, *84*, 6059-6069, 1979.
- [70] Jeanloz, R., The nature of the Earth's core, *Annu. Rev. Earth Planet. Sci.*, *18*, 357-386, 1990.
- [71] Jeanloz, R., and T. J. Ahrens, Equations of state of FeO and CaO, *Geophys. J. R. Astron. Soc.*, *62*, 505-528, 1980.
- [72] Jeanloz, R., and S. Morris, Temperature distribution in the crust and mantle, *Annu. Rev. Earth Planet. Sci.*, *14*, 377-415, 1986.
- [73] Jeanloz, R., and H.-R. Wenk, Convection and anisotropy of the inner core, *Geophys. Res. Lett.*, *15*, 72-75, 1988.
- [74] Jephcoat, A. and P. Olson, Is the inner core of the Earth pure iron, *Nature*, *325*, 332-335, 1987.
- [75] Jephcoat, A. P., H.-K. Mao, and P. M. Bell, Static compression of iron to 78 GPa with rare gas solids as pressure-transmitting media, *J. Geophys. Res.*, *91*, 4677-4684, 1986.
- [76] Karato, S.-I., Inner core anisotropy due to the magnetic field induced preferred orientation of iron, *Science*, *262*, 1708-1710, 1993.
- [77] Karato, S.-I., Seismic anisotropy of the Earth's inner core resulting from flow induced by Maxwell stresses, *Nature*, *402*, 871-873, 1999.
- [78] Karato, S.-I., and V. R. Murthy, Core formation and chemical equilibrium in the Earth - I. Physical considerations, *Phys. Earth Planet. Inter.*, *100*, 61-79, 1997.
- [79] Kohn, W., and L. J. Sham, Self-consistent equations including exchange and correlation effects, *Phys. Rev.*, *140*, A1133-1138, 1965.
- [80] Körling, M., and J. Häglund, Cohesive and electronic properties of transition metals: the generalized gradient method, *Phys. Rev. B* *45*, 13293-13297, 1992.
- [81] Kuang, W., and J. Bloxham, An Earth-like numerical dynamo model, *Nature*, *389*, 371-374, 1997.
- [82] Laio, A., S. Bernard, G. L. Chiarotti, S. Scandolo, and E. Tosatti, Physics of iron at Earth's core conditions, *Science*, *287*, 1027-1030, 2000.
- [83] Laske, G., and G. Masters, Rotation of the inner core from a new analysis of free oscillations, *Nature*, *402*, 66-69, 1999.
- [84] Lehmann, I., P', *Bur. Cent. Seismol. Int. A*, *14*, 3-31, 1936.
- [85] Li, J., and C. B. Agee, Geochemistry of mantle-core differentiation at high pressure, *Nature*, *381*, 686-689, 1996.
- [86] Lübbbers, R., H. F. Grünstedel, A. I. Chumakov, and G. Wortmann, Density of phonon states in iron at high pressure, *Science*, *287* 1250-1253, 2000.
- [87] Lundqvist, S., and N. H. March, *Theory of the inhomogeneous electron gas*, 395 pp., Plenum Press, New York, 1983.
- [88] Manghnani, M. H., K. Katahara, and E. S. Fisher, Ultrasonic equation of state of rhenium, *Phys. Rev. B* *9*, 1421-1431, 1974.
- [89] Mao, H.-K., Y. Wu, L. C. Chen, J. F. Shu, and A. P. Jephcoat, Static compression of iron to 300 GPa and Fe<sub>0.8</sub>Ni<sub>0.2</sub> alloy to 260 GPa: Implications for the composition of the core, *J. Geophys. Res.*, *95*, 21737-21742, 1990.
- [90] Mao, H.-K., J. Shu, G. Shen, R. J. Hemley, B. Li, and A. K. Sing, Elasticity and rheology of iron above 220 GPa and the nature of the Earth's inner core, *Nature*, *396*, 741-743, 1998. Correction, *Nature*, *399*, 280, 1999.
- [91] Mao, H.-K., J. Xu, V. V. Struzhkin, J. Shu, R. J. Hemley, W. Sturhahn, M. Y. Hu, E. E. Alp, L. Vočadlo, D. Alfè, G. D. Price, M. J. Gillan, M. Schwoerer-Böhning, D. Häusermann, P. Eng, G. Shen, H. Giefers, R. Lübbbers, and G. Wortmann, Phonon density of states of iron up to 153 Gigapascals, *Science*, *292*, 914-916, 2001.
- [92] Masters, G., Observational constraints on the chemical and thermal structure of the Earth's deep interior, *Geophys. J. R. Astron. Soc.*, *57*, 507-534, 1979.
- [93] Masters, G., and F. Gilbert, Structure of the inner core inferred from observations of its spheroidal shear modes, *Geophys. Res. Lett.*, *8*, 569-571, 1981.
- [94] Matsui, M., and O. L. Anderson, The case for a body-centered cubic phase ( $\alpha'$ ) for iron at inner core conditions, *Phys. Earth Planet. Inter.*, *103*, 55-62, 1997.
- [95] Matthies, S., S. Merkel, H.-R. Wenk, R. J. Hemley, and H.-K. Mao, Effects of texture on the determination of elasticity of polycrystalline  $\epsilon$ -iron from diffraction measurements, *Earth Planet. Sci. Lett.*, *194*, 201-212, 2001.
- [96] Maurer, M., M. Piecuch, M. F. Ravet, J. C. Ousset, J. P. Sanchez, C. Aaron, J. Dekoster, D. Raoux, A. Desandres, M. Desantis, A. Fontaine, F. Baudelet, J. L. Rouviere, and B. Dieny, Magnetism and structure in hexagonal Fe/Ru superlattices with short periodicity, *J. Magn. Magn. Mater.*, *93*, 15-24, 1991.
- [97] McMahon, A. K., and M. Ross, High-temperature electron-band calculations *Phys. Rev. B* *15*, 718-725, 1977.
- [98] Merkel, S., A. F. Goncharov, H.-K. Mao, P. Gillet, and R. J. Hemley, Raman spectroscopy of iron to 152 GPa: Implications for Earth's inner core, *Science*, *288*, 1626-1629, 2000.
- [99] Merrill, R. T., M. W. McElhinny, and P. L. McFadden, *The magnetic field of the Earth*, 531 pp., Academic Press, San Diego, CA, 1996.
- [100] Morelli, A., A. M. Dziewonski, and J. H. Woodhouse, Anisotropy of the inner core inferred from PKIKP travel times, *Geophys. Res. Lett.*, *13*, 1545-1548, 1986.
- [101] Moroni, E. G., G. Grimvall, and T. Jarlborg, Free energy contributions to the hcp-bcc transformation in transition metals, *Phys. Rev. Lett.* *76*, 2758-2761, 1996.
- [102] Nguyen, J. H., and N. C. Holmes, Iron sound velocity and its implications for the iron phase diagram, *submitted to Science*, 2001.
- [103] Nielsen, O. H., and R. M. Martin, Quantum-mechanical theory of stress and force, *Phys. Rev. B* *32*, 3780-3791, 1985.
- [104] Niu, F., and L. Wen, Hemispherical variations in seismic velocity at the top of the Earth's inner core, *Nature*,

- 410, 1081-1084, 2001.
- [105] Okal, E. A., and Y. Cansi, Detection of PKJKP at intermediate periods by processing multichannel correlation, *Earth Planet. Sci. Lett.*, *164*, 23-30, 1998.
- [106] Okuchi, T., Hydrogen partitioning into molten iron at high pressure: implications for Earth's core, *Science*, *278*, 1781-1784, 1997.
- [107] Olijnyk, H., and A. P. Jephcoat, Optical zone-center phonon modes and macroscopic elasticity in hcp metals, *Solid State Communications*, *115*, 335-339, 2000.
- [108] Olijnyk, H., A. P. Jephcoat, and K. Refson, On optical phonons and elasticity in the hcp transition metals Fe, Ru and Re at high pressure, *Europhysics Letters*, *53*, 504-510, 2001.
- [109] Parrinello, M., and A. Rahman, Strain fluctuations and elastic constants, *J. Chem. Phys.*, *76*, 2662-2666, 1982.
- [110] Perdew, J. P., K. Burke, and M. Ernzerhof, Generalized Gradient Approximation Made Simple, *Phys. Rev. Lett.* *77*, 3865-3868, 1996. Correction, *Phys. Rev. Lett.* *78*, 1396, 1997.
- [111] Pickett, W. E., Pseudopotential methods in condensed matter applications, *Comp. Phys. Rep.*, *9*, 115-197, 1989.
- [112] Poirier, J. P., Light elements in the Earth's outer core - a critical review, *Phys. Earth Planet. Inter.*, *85*, 319-337, 1994.
- [113] Poirier, J. P., and G. D. Price, Primary slip system of  $\epsilon$ -iron and anisotropy of the Earth's inner core, *Phys. Earth Planet. Inter.*, *110*, 147-156, 1999.
- [114] Poupinet, G., R. Pillet, and A. Souriau, Possible heterogeneity of the Earth's core deduced from PKIKP travel times, *Nature*, *305*, 204-206, 1983.
- [115] Saxena, S. K., L. S. Dubrovinsky, P. Haggkvist, Y. Cerenius, G. Shen, and H.-K. Mao, Synchrotron X-ray study of iron at high-pressure and temperature, *Science*, *269*, 1703-1704, 1995.
- [116] Shearer, P. M., Constraints on inner core anisotropy from ISC PKP(DF) travel-times, *J. Geophys. Res.*, *99*, 19647-19659, 1994.
- [117] Shen, G., and D. L. Heinz, High pressure melting of deep mantle and core materials, *Reviews in Mineralogy*, *37*, 369-396, 1998.
- [118] Shen, G., H.-K. Mao, R. J. Hemley, T. S. Duffy, and M. L. Rivers, Melting and crystal structure of iron at high pressures and temperatures, *Geophys. Res. Lett.*, *25*, 373-376, 1998.
- [119] Simmons, G., and H. Wang, *Single crystal elastic constants and calculated aggregate properties: a handbook*, 370 pp., M. I. T. Press, Cambridge, Mass., 1971.
- [120] Singh, A. K., C. Balasingh, H.-K. Mao, J. Shu, and R. J. Hemley, Analysis of lattice strains measured under nonhydrostatic pressure, *J. Appl. Phys.*, *83*, 7567-7575, 1998a.
- [121] Singh, A. K., H.-K. Mao, J. Shu, and R. J. Hemley, Estimation of single-crystal elastic moduli from polycrystalline X-ray diffraction at high pressure: application to FeO and iron, *Phys. Rev. Lett.* *80*, 2157-2160, 1998b.
- [122] Singh, D. J., *Planewaves, pseudopotentials and the LAPW method* 115 pp., Kluwer Academic Publishers, Dordrecht, 1994.
- [123] Singh, S. C. , M. A. J. Taylor, and J. P. Montagner, On the presence of liquid in Earth's inner core, *Science*, *287*, 2471-2474, 2000.
- [124] Söderlind P., J. A. Moriarty, and J. M. Wills, First-principles theory of iron up to Earth-core pressures: Structural, vibrational, and elastic properties, *Phys. Rev. B* *53*, 14063-14072, 1996.
- [125] Song, X. D., Anisotropy of Earth's inner core, *Rev. Geophys.*, *35*, 297-313, 1997.
- [126] Song, X. D., and D. V. Helmberger, Anisotropy of the Earth's inner core, *Geophys. Res. Lett.*, *20*, 2591-2594, 1993.
- [127] Song, X. D., and D. V. Helmberger, Depth dependence of anisotropy of Earth's inner core, *J. Geophys. Res.*, *100*, 9805-9816, 1995.
- [128] Song, X. D., and D. V. Helmberger, Seismic evidence for an inner core transition zone, *Science*, *282*, 924-927, 1998.
- [129] Song, X. D., and P. G. Richards, Seismological evidence for differential rotation of the Earth's inner core, *Nature*, *382*, 221-224, 1996.
- [130] Souriau, A., New seismological constraints on differential rotation rates of the inner core from Novaya Zemlya events recorded at DRV, Antarctica, *Geophys. J. Int.*, *134*, F1-5, 1998.
- [131] Stacey, F. D., *Physics of the Earth*, 513 pp., Brookfield Press, Brisbane, 1992.
- [132] Steinle-Neumann, G., L. Stixrude, and R. E. Cohen, First-principles elastic constants for the hcp transition metals Fe, Co, and Re at high pressure, *Phys. Rev. B* *60*, 791-799, 1999.
- [133] Steinle-Neumann, G., L. Stixrude, R. E. Cohen, and O. Gülseren, Elasticity of iron at the temperature of Earth's inner core, *Nature*, *413*, 57-60, 2001.
- [134] Stixrude, L., Elastic constants and anisotropy of MgSiO<sub>3</sub> perovskite, periclase, and SiO<sub>2</sub> at high pressure, in *The Core-Mantle Boundary Region, Geodynamic Series 28*, edited by M. Gurnis et al., pp. 83-96, American Geophysical Union, Washington, DC, 1998.
- [135] Stixrude, L., and J. M. Brown, The Earth's core, *Rev. Mineralogy*, *37*, 261-280, 1998.
- [136] Stixrude, L., and R. E. Cohen, Constraints on the crystalline structure of the inner core - mechanical instability of bcc iron at high-pressure, *Geophys. Res. Lett.*, *22*, 125-128, 1995a.
- [137] Stixrude, L., and R. E. Cohen, High-pressure elasticity of iron and anisotropy of Earth's inner-core, *Science*, *267*, 1972-1975, 1995b.
- [138] Stixrude, L., R. E. Cohen, and D. J. Singh, Iron at high pressure: Linearized-augmented-plane-wave computations in the generalized-gradient approximation, *Phys. Rev. B* *50*, 6442-6445, 1994.
- [139] Stixrude, L., E. Wasserman, and R. E. Cohen, Composition and temperature of Earth's inner core, *J. Geophys. Res.*, *102*, 24729-24739, 1997.
- [140] Su, W.-J., and A. M. Dziewonski, inner core anisotropy in three dimensions, *J. Geophys. Res.*, *100*, 9831-9852, 1995.
- [141] Su, W.-J., A. M. Dziewonski, and R. Jeanloz, Planet within a planet: Rotation of the inner core of the Earth, *Science*, *274*, 1883-1887, 1996.
- [142] Tanaka, S., and H. Hamaguchi, Degree one heterogeneity and hemispherical variation of anisotropy in the inner core from PKP(BC)-PKP(DF) times, *J. Geophys. Res.*, *102*, 2925-2938, 1997.
- [143] Taylor, R. D., M. P. Pasternak, and R. Jeanloz, Hysteresis in the high-pressure transformation of bcc-iron to hcp-iron *J. Appl. Phys.*, *69*, 6126-6128, 1991.

- [144] Tromp, J., Support for anisotropy of the Earth's inner core from free oscillations, *Nature*, *366*, 678-681, 1993.
- [145] Tromp, J., Inner-core anisotropy and rotation, *Annu. Rev. Earth Planet. Sci.*, *29*, 47-69, 2001.
- [146] Troullier, N., and J. L. Martins, Efficient pseudopotentials for plane-wave calculations, *Phys. Rev. B* *43*, 1993-2006, 1991.
- [147] Tsunoda, Y., Y. Nishioka, and R. M. Nicklow, Spin fluctuations in small  $\gamma$ -Fe precipitates, *J. Magn. Magn. Mater.*, *128*, 133-137, 1993.
- [148] Uchida, T., Y. Wang, M. L. Rivers, and S. R. Sutton, Stability field and thermal equation of state of  $\epsilon$ -iron determined by synchrotron X-ray diffraction in a multianvil apparatus, *J. Geophys. Res.*, *106*, 21799-21810, 2001.
- [149] Uhl, M., L. M. Sandratskii, and J. Kübler, Spin fluctuations in  $\gamma$ -Fe and Fe<sub>3</sub>Pt Invar from local-density-functional calculations, *Phys. Rev. B* *50*, 291-301, 1994.
- [150] Verhoogen, J., Heat balance of the Earth's core, *Geophys. J. R. Astron. Soc.*, *4*, 276-281, 1961.
- [151] Verhoogen, J., *Energetics of the Earth*, 139 pp., National Academy of Sciences, Washington, DC, 1980.
- [152] Vidale, J. E., and P. S. Earle, Fine scale heterogeneity in the Earth's inner core, *Nature*, *406*, 273-275, 2000.
- [153] Vočadlo, L., J. Brodholt, D. Alfè, M. J. Gillan, and G. D. Price, Ab initio free energy calculations on the polymorphs of iron at core conditions. *Phys. Earth Planet. Inter.*, *117*, 123-137, 2000.
- [154] Wasserman, E., L. Stixrude, and R. E. Cohen, Thermal properties of iron at high pressures and temperatures, *Phys. Rev. B* *53*, 8296-8309, 1996.
- [155] Watt, J. P., and L. Peselnick, Clarification of the Hashin-Shtrikman bounds on the effective elastic moduli of polycrystals with hexagonal, trigonal, and tetragonal symmetry, *J. Appl. Phys.*, *51*, 1525-1531, 1980.
- [156] Wenk, H.-R., T. Takeshita, R. Jeanloz, and G. C. Johnson, Development of texture and elastic-anisotropy during deformation of hcp metals, *Geophys. Res. Lett.*, *15*, 76-79, 1988.
- [157] Wenk, H.-R., J. R. Baumgardner, R. A. Lebensohn, and C. N. Tomé, A convection model to explain anisotropy of the inner core, *J. Geophys. Res.*, *105*, 5663-5677, 2000a.
- [158] Wenk, H.-R., S. Matthies, R. J. Hemley, H.-K. Mao, and J. Shu, The plastic deformation of iron at pressures of the Earth's inner core, *Nature*, *405*, 1044-1046, 2000b.
- [159] Wentzcovitch, R. M., Invariant molecular-dynamics approach to structural phase transitions, *Phys. Rev. B* *44*, 2358-2361, 1991.
- [160] de Wijs, G. A., G. Kresse, L. Vočadlo, D. Dobson, D. Alfè, M. J. Gillan, and G. D. Price, The viscosity of liquid iron at the physical conditions of the earth's core, *Nature*, *392*, 805-807, 1998.
- [161] Williams, Q., R. Jeanloz, J. Bass, B. Svendsen, and T. J. Ahrens, The melting curve of iron to 250 gigapascals - a constraint on the temperature at Earth's center, *Science*, *236*, 181-182, 1987.
- [162] Woodhouse, J. H., D. Giardini, and X. D. Li, Evidence for inner core anisotropy from free oscillations, *Geophys. Res. Lett.*, *13*, 1549-1552, 1986.
- [163] Yagi, T., K. Fukuoka, H. Takei, and Y. Syono, Shock compression of wüstite, *Geophys. Res. Lett.*, *15*, 816-819, 1988.
- [164] Yoo, C. S., N. C. Holmes, M. Ross, D. J. Webb, and C. Pike, Shock temperatures and melting of iron at Earth core conditions, *Phys. Rev. Lett.* *70*, 3931-3934, 1993.
- [165] Yoo, C. S., J. Akella, A. J. Campbell, H.-K. Mao, and R. J. Hemley, Phase-diagram of iron by in-situ x-ray-diffraction - implications for Earth core, *Science*, *270*, 1473-1475, 1995.
- [166] Yoshida, S., I. Sumita, and M. Kumazawa, Growth model of the inner core coupled with outer core dynamics and the resultant elastic anisotropy. *J. Geophys. Res.*, *101*, 28085-28103, 1996.
- [167] Yukutake, T., Implausibility of thermal convection in the Earth's solid inner core, *Phys. Earth Planet. Inter.*, *108*, 1-13, 1998.
- [168] Yukutake, T., The inner core and the surface heat flow as clues to estimating the initial temperature of Earth's core, *Phys. Earth Planet. Inter.*, *121*, 103-137, 2000.